SCIENTIFIC & TECHNICAL REPORTS SUMMARY
FINAL REPORT

Contractor
J.A. Woollam Co., Inc.
645 M Street, Suite 102
Lincoln, NE 68508

Title of Work
Spacecraft Thermal Control Management Using Electrochromatics
Contract Number
DASG60-98-C-0054

Contracting Period
February 2nd, 1998 to February 1st, 2000

Sponsored by
ARPA/BMDO Innovative Science and Technology Office
7100 Defense Pentagon
Washington, DC 20301-7100

Managed by

U.S. Army Strategic Defense Command

Reported by
Principal Scientist: John A. Woollam
402/477-7501

Submitted
02-01-2000

FINAL REPORT ON PHASE II:
Covering two year BMDO SBIR contract number: #DASG60-98-C-0054

Spacecraft Thermal Control Management Using Electrochromics

Submitted by:
Chris Trimble[a], Eve Franke[a], Jeff Hale [b], Mick DeVries[a], and John A. Woollam[a,b]

[a]Center for Microelectronics and Optical Materials Research
University of Lincoln-Nebraska
Electrical Engineering Dept
209N WSEC
Lincoln, NE 68588

[b]J.A. Woollam Co., Inc
645 "M" Street
Lincoln, NE 68508

January 31, 2000

REPORT DOCUMENTATION PAGE **Contract No. DASG60-98-C-0054**				Form Approved OMB No. 0704-0188
1a. REPORT SECURITY CLASSIFICATION **Unclassified, no security requirements**			1b. RESTRICTIVE MARKINGS **NONE**	
2a. SECURITY CLASSIFICAITON AUTHORITY **UNCL**			3. DISTRIBUTION AVAILABILITY REPORT **Unlimited for public release**	
2b. DECLASSIFICAITON DOWNGRADING SCHEDULE **UNCL**				
4. PERFORMING ORGANIZATION REPORT NUMBERS **CLIN 0002-A002 Scienfic & Technical Summary Final Report, DOC# DI-MISC-80048/M**			5. MONITORING ORGANIZATION REPORT NUMBERS **CLIN 0002-A002 Scienfic & Technical Summary Final Report, DOC# DI-MISC-80048/M**	
6a.NAME OF PERFORMING ORGANIZATION **J.A. Woollam Co., Inc.**	6b.OFFICE SYMBOL **JAW CO**		7a. NAME OF MONITORING ORGANIZATION **U.S. Army Space and Missile Defense Command**	
6c. ADDRESS (City, State and Zip Code) **645 M Street, Suite 102 Lincoln, NE 68508**			7b. ADDRESS (Ciry, State and ZIP Codes) **PO Box 1500, ATTN: SMDC-PA Huntsville, AL 65807-3801**	
8a. NAME OF FUNDING/SPONSORING ORGANIZATION **Ballistic Missile Defense Organization**	8b.OFFICE SYMBOL (if applicable) **BMDO**		9.PROCUREMENT INSTRUMENT IDENTIFICATION NO. **DOC#: DI-MISC-80048/M Contract No. DASG60-98-C-0054**	
8c. ADDRESS (City, State and Zip Code) **7100 Defense, Pendegon Roo, 1E 167 Washington, DC 20301-7100**			10. SORCE OF FUNDING NUMBERS	
			PROGRAM ELEMENT NO.	PROJECT NO. / TASK NO. / WORK UNIT ACCESSION NO. **DPPH**
11. TITLE (includes Seciruty Classification) **Spacecragt Thermal Control Management Using Electrochromics (Unclassified)**				
12. PERSONAL AUTHOR(S) **Jeff Hale (PI), Chris Trimble, PI of subcontractor and John A. Woollam., president**				
13a TYPE OF REPORT **Final Scientific and Technical Report**	13b.TIME COVERED **FROM 2-2-98 T 2-1-2000**	14. DATE OF REPORT (Year, Month, Day) **2000/02/01 (Feb. 1st, 2000)**	15. PAGE COUNT **64**	
16. SUPPLYMENTARY NOTATION **Prepared in cooperation with subcontractor, the University of Nebraska, Lincoln**				
17. COSATI CODES FIELD / GROUP / SUB-GROUP			18.SUBJECT TERMS (continue on reverse if necessary & identify by block numbe **Variable-emissivity coatings, Spacecraft thermal control Infrared-electrochromics**	
19. ABSTRACT (continue on reverse if necessary and identify by block number) **Thin-film multilayer electrochromic coatings for thermal control of spacecraft were designed, built and tested. Design was for a 300°K spacecraft. but coatings would also work well for warmer surface emittance control. Changes in emissivity of dE=0.2, and ratios of "on" to "off" emissivity were as high as 3.5. Further work is needed to improve reproducibility of results and long-term stability.**				
20. DISTRIBUTION AVAILABILITY OF ABSTRACT **Unlimited**			21. ABSTRACT SECURITY CLASSIFICATION **Unclassified**	
22a. NAME OF RESPONSIBLE INDIVIDUAL **JEFF HALE, PI, J.A. Woollam Co., Inc.**			22b. TELEPHONE (include Area Code) **402/477-7501 Ext. 226**	22.OFFICE SYMBO **JAWCO**

DD Form 1473, JUN 87

PART I: INTRODUCTION

Current techniques of thermal control of spacecraft are based on metallic blinds mounted on a highly IR emissive backplate. Electrochromic devices have been investigated as potential replacements for this technology.

These devices are composed of thin films that change their optical properties under the action of a small applied voltage. There are several potential benefits of applying an electrochromic coating to this task. This type of device has no moving parts and failures due to mechanical wear would be eliminated. The second benefit of utilizing this device is its lightweight; a stack of thin films would not add significant weight to the satallite.

The energy balance equation for a craft in low earth orbit is given as follows:

Energy emitted by satallite = Energy generated by internal electrical components + albedo + earthshine

Energy Out Energy In

Albedo is the sunlight reflected from the earth's surface, this contributes the majority of the heat to the satallite.

Earthshine is the infrared radiation emitted from the earth. The earth is closely approximated as a 0°C blackbody. This needs to be accounted for because the emitted wavelengths are very similar to those being emitted from the satellite. This means that as the satellite radiators are activated the earthshine will be absorbed.

There are two ways to utilize an electrochromic device in a thermal control surface. One way is to deposit the layers onto an IR black (emissive) substrate. In this case the reflectivity of the top electrochromic layer is contrasted with the emissive substrate. When the top layer is intercalated the device becomes much more IR reflective and this corresponds to the low emittance state of the device. This is analogous to having the venetion blinds closed on the mechanical thermal control system. When the switching voltage is applied the ions move from the top layer and into the storage layer, bringing about an optical change that makes the device more IR transparent. This allows the emissive substrate to radiate the energy out of the thermally controlled surface.

The drawback to this use of electrochromics is the requirement for an electrical conductor that could cover the emissive substrate without adversely affecting the substrates emissivity. The best way to accomplish this is to utilize a conducting grid on the bottom of the device as well as the top optically switching layer. This would require an additional step in the process of fabricating a device.

The second way to use an electrochromic is to deposit the device on a highly reflective substrate. In this case when the top layer is intercalated the efficiency with which the device reflects IR radiation is dramatically decreased. This has the effect of increasing the emissivity of the surface when the optically switching layer is intercalated. By using this method the substrate can also act as an electrical conductor for the device. This is how we fabricated our devices.

A simple schematic of the electrochromic device developed on this contract is shown in Figure 1.

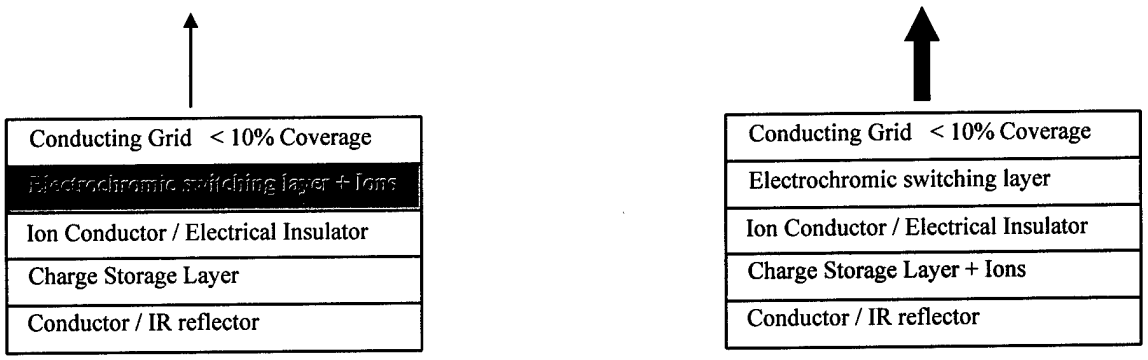

Figure 1: An electrochromic device a) in the high emittance state with ions intercalated into the optically switching top layer b) in the high reflectance state with ions intercalated into the charge

A. CONTRACT OBJECTIVES

There were several objectives and associated work tasks of this phase II SBIR contract. In Phase I the first devices were fabricated. These utilized H^+ ion as the mobile charging species, and a polymer as the ion conductor.

One primary goal of this Phase II contract was to improve the performance of this device and increase the spectral range of its operation. Several things have been implemented in order to achieve this goal. The performance improvements will be demonstrated in Part III of this report. In one case an antireflection coating of DLC on a low-dopant concentration Si substrate was used. We also utilized in-situ ellipsometric monitoring during film growth to improve control of layer thickness. The third improvement was to adjust the deposition conditions of sputtered c-WO_3 in order to increase the crystallinity of the material.

Another important goal of the contract was to extend the optical measurements out to 30 microns. The J.A. Woollam Co. has developed a line of ellipsometers that can make measurements at wavelengths greater than 35 microns. This contract helped develop this technology, and several of these instruments were built and shipped to commercial customers. That is, there was a rapid commercialization.

In order to increase the feasibility of profitable manufacture of electrochromic devices for spacecraft thermal control, a dry method of intercalation was also explored. A Lithium evaporation technique was successfully used to reversibly intercalate cWO_3 samples. The details and results of using this system can be found in the 1999 fourth quarterly contract report. Another benefit of utilizing a dry intercalation technique is that monolithic electrochromic devices can be made. This has eliminated the need for polymeric ion conductors, which have many optical absorption lines in the infrared, which reduce emissivity modulation. The thickness needed for a non-organic vacuum deposited ion conductor is also much less than for a polymeric ion conductor.

Investigating film uniformity was also a goal in this contract, and small-scale topographical studies were done in order to quantify the nonuniformity of several of these films.

The geometric configuration, and the relative distance between the substrate and sputtering targets have the greatest effects on uniformity of depositions. The sputtering system we employed for making our thin films did not have the freedom of altering these deposition conditions without major mechanical re-design. The uniformity of the films was good in the center of the substrates, and this is the region where devices were fabricated, and measurements on single films were made.

Another objective of this contract was to make a working device on a non-planer surface, and to make uniform devices with large area surfaces. Due to the difficulty of developing reliable devices on small planer surfaces and the problems posed by shaped surfaces and large area devices, no attempt was made to make large area, curved surface devices.

Long-term device stability was also a major goal of the program. This was the most difficult challenge of the contract, and was a major part of the work. Many ideas were implemented in order to improve long-term device operation.

One of these was to switch from H^+ ions (used in Phase I) to Li^+ ions for the majority of the work done in Phase II. H^+ has a high ion diffusion constant in many of the materials we investigated. This allows the small ion to leave the device much more rapid relative to Li^+. We were able to increase the "shelf life" of our devices by utilizing Li^+ as the intercalant species. Another benefit of using Li^+ is that the electrochemical solution is an organic. This is ideal because some of the materials under study were not compatible with aqueous solutions.

A systematic investigation was made on the switching voltages needed for best device operation. The applied voltages were systematically increased, for each of the different devices, so as to induce a color change. By using minimum switching voltages it was more certain that any device failures were not caused by electrical damage to the devices.

Finally, different non-organic ion conductors were evaluated for replacement of the polymer, which seemed to degrade after several emittance-switching cycles. The ion conductors are a critical problem in development of reliable working devices. A good ion conductor will have two important characteristics. First, it must be electrically insulating, and second the mobile ion species needs to have good diffusivity in the lattice. The lattice defects necessary for ion mobility also provide potential electrical shorts through the material. The density of the ion-conductor needs to be optimized so it can possess both properties. Considerable work was done to optimize TaOx for this purpose.

The following sections give more details of the work done during this contract.

B. BACKGROUND ON DEVICE OPERATION

Before going into the performance of the devices we have made during this contract it will be beneficial to review some of the important ideas. The first of which is the conversion of a reflectivity measurement to an emissivity measurement. Any radiation that is incident on a sample will be transmitted, reflected or absorbed. For a blackbody the absorbed component is also the radiation that will be emitted. If no light is transmitted through a sample then the measured reflectance is easily converted to absorbance or emittance by subtracting from unity. This assumes that all reflection is specular, that is, no light is scattered.

The way an electrochromic device, which is based on a tungsten oxide film, works is shown by way of a fairly straightforward Red-Ox reaction equation:

$$\mathbf{WO_3 + xM^+ + xe^- \leftrightarrow M_xWO_3}$$

Lower Emittance	Higher Emittance
Higher Reflectance	Lower reflectance

$$\mathbf{M = H^+, Li^+, Na^+, or\ K^+}$$

In the work done on this contract we utilized both H^+ and Li^+ ions. The reaction above applies to the crystalline WO_3 top layer, and also to the amorphous WO_3 layer in some devices.

In order to determine how well the devices performed, Plank's blackbody equation was used. This equation was then used to weight the reflection curves of the device in its two states. The following equations were utilized:

$$M(\sigma, T) = 2\pi h c \sigma^3 \times \frac{1}{e^{\left(hc\sigma/kT\right)} - 1} \qquad (1)$$

Where h is Planck's constant, c is the speed of light, σ is the frequency of light, and k is Boltzmann's constant. Figure 1 shows the results of using 298K (Room Temperature) for T. This yields the emittance of a room temperature blackbody.

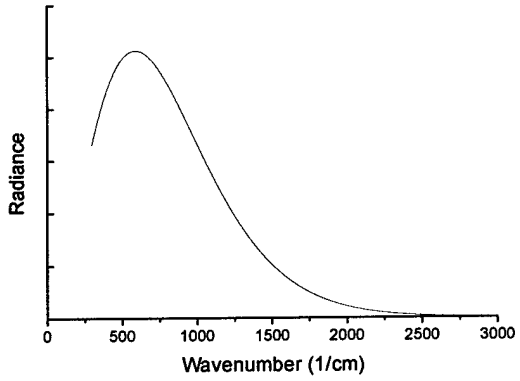

Figure 1: Blackbody radiance spectra for 298K blackbody.

This shows the spectral region needed to optically modulate the device for thermal control of a system that is to be maintained at Room temperature.

In order to calculate relative figure of merit for performance of the devices we used the reflectance curves obtained from measurements on devices. These curves were then multiplied with the blackbody equation at each wavelength of the blackbody spectrum seen in Figure 1. This product was integrated over all wavelengths and divided by the blackbody integral. This calculation is shown as

$$\text{Emittance} = \frac{\int(1 - \text{Reflectance}) \times M(\sigma, T)d\sigma}{\int M(\sigma, T)d\sigma} \qquad (2)$$

PART II: MATERIALS

A. Polycrystalline Tungsten Oxide

In electrochromic devices for visible operation amorphous tungsten oxide is commonly used as the main electrochromic switching material. The optical properties of amorphous tungsten oxide are not compatible with efficient infrared switching. Thus considerable effort on this contract was spent preparing optimized polycrystalline films of tungsten oxide.

Polycrystalline Tungsten Oxide (cWO_{3-z}) contributes the majority of the infrared optical switching. The intercalated oxide is more IR reflective than the unintercalated oxide. This change is due to the intercalant ions (either H^+ or Li^+) acting as free carriers in the WO_{3-z} lattice. When the device is deposited on top of an emissive substrate then the reflectivity of the top layer contrasts with the emittance of the bottom layer and this causes a lower emittance when the cWO_{3-z} is intercalated. In the work done here the devices have been deposited on highly reflective substrates (Gold, Chrome, Aluminum or Indium Tin Oxide (ITO)). However as will be shown in the following sections many of the materials used in the device have optical absorptions caused by lattice effects. These lattice absorptions are at the same region as the peak of the blackbody and this has the same effect as depositing the cWO_{3-z} on an emissive material.

The key to device operation is that the cWO_{3-z} is on top of the stack and as exposed as possible to the ambient environment. A normal electrochromic device has two transparent electrical conductors, as in Figure 1 of previous section. These conducting layers are infrared reflectors due to the free carriers inherent in electron conductors. For this reason the exposed electrochromic layer will need to utilize a grid structure for the top electrical conductor.

In order to confirm that the films are polycrystalline, X-Ray Diffraction (XRD) measurements were taken on films deposited at various temperatures. Figure 2 shows how XRD peaks from polycrystalline WO_{3-z} appear and grow as deposition temperature increases. Peaks due to polycrystalline material appear only at 300° and 400° C (top two curves).

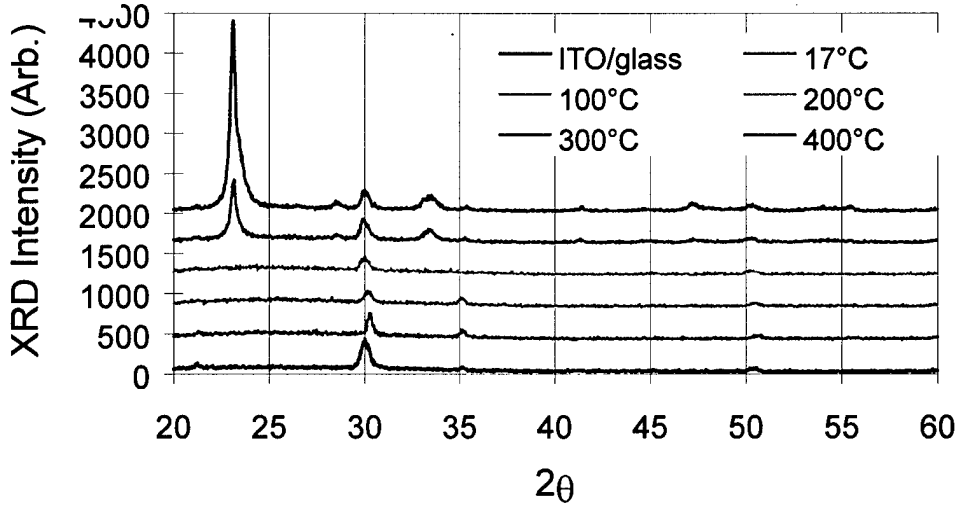

Figure 2: XRD Data Aquired from samples of WO_{3-z} deposited at various temperatures.

Several benefits arise from using cWO_{3-Z} as the main electrochromic layer. This material has good infrared coloring efficiency. This is a measure of the change in optical density per unit of charge (ions) inserted into the material. The coloring efficiency (CE) is calculated as follows:

$$CE = \frac{\Delta OD}{Q_{in}}$$

$$\Delta OD = \log\left(\frac{T_{Bleached}}{T_{Colored}}\right)$$

$$Q_{in} = \frac{Current \times Time}{Intercalation\ area\ of\ the\ film}$$

Where OD is optical density, and Q is the charge per unit area entering the film.

In order to investigate coloring efficiency of c-WO_3, transmission measurements were made on films deposited on IR transparent Si substrates. Figure 3a shows transmission measurements of the colored (intercalated) and bleached (unintercalated) states. The amount of charge inserted into the films was calculated by holding the current constant for a fixed amount of time, and specifying the area of the film that was colored. Figure 3b) shows the calculated coloring efficiency based on the calculated charge inserted, and the change in transmission after the ions had been inserted.

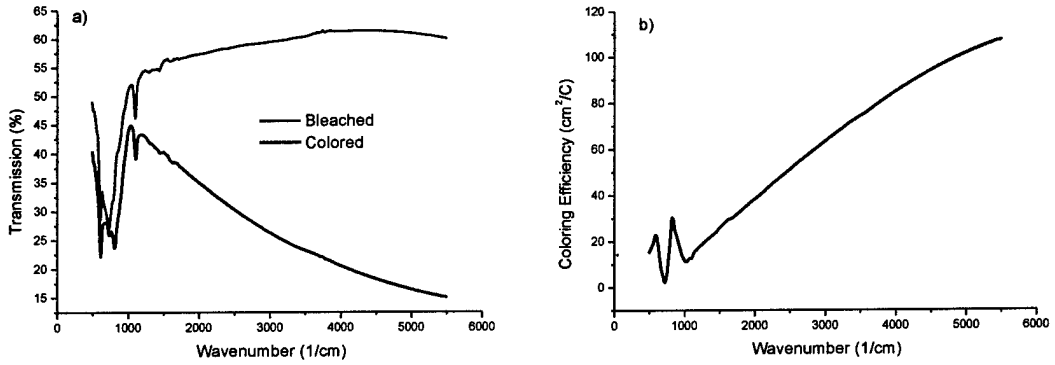

Figure 3: a)Transmission of c-WO_3 on infrared (IR) transparent Si. The films were colored with a current of 2mA for 21seconds. b) Calculated coloring efficiency, from the transmission measurements, of c-WO_3 on IR transparent Si.

These Coloring Efficiency results were reproducible from one sample to the next. However, most samples have been switched by holding the voltage constant, that is, the current was not measured. Without having the measurement of the electrical current it is not possible to count the charge moving in and out of the films.

Figure 4a shows the transmission measurements made on another c-WO_3 sample that was switched in this manner. 4b shows the plot of ΔOD from these measurements. The ΔOD has the same shape and features as the coloring efficiencies of the above sample. If we assume a Q_{in} of 0.01 Coulombs/cm^2 (3.5mA for 21 seconds) the two curves lie almost on top of one another. Figure 4c compares the two samples.

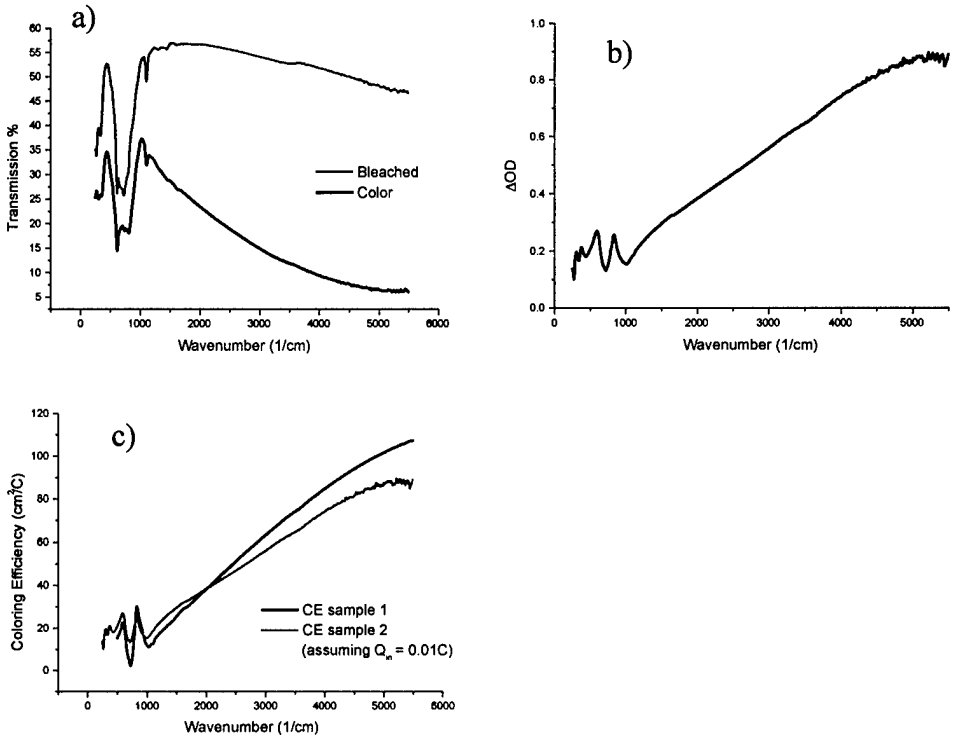

Figure 4: a) Transmission of c-WO_3 on infrared (IR) transparent Si. Films were colored by holding the voltage applied to the films at –1.0V to color and +1.0V to bleach. b) Calculated ΔOD, from the transmission measurements c) comparison of CE between two samples assuming a current of 3.5mA was applied to sample two for 21 seconds.

Another benefit of utilizing tungsten oxide is that it is easily sputtered from a metal target in a gas of mixed Ar and O_2. Of the many thin film deposition techniques available, reactive magnetron sputtering lends itself to scaling up to large area surfaces.

Another advantage that c-WO_3 provides is the durability it has in both aqueous and non-aqueous solutions. This allows intercalation studies to be done with either H^+ or Li^+ ions.

In order to determine the thickness of the films, fast spectroscopic ellipsometric data were acquired during deposition. This provided a means of determining the growth rate of the films. After the growth rate was determined, the duration of subsequent depositions was recorded and film thickness could be ascertained. Figure 5 shows the results of an example of such a measurement (For a complete tabulation se DeVries Thesis, JVST). The deposited films were modeled as simple transparent films. The experiment is especially sensitive to the beginning and end of the deposition. These points are especially important in determination of growth rate and thickness.

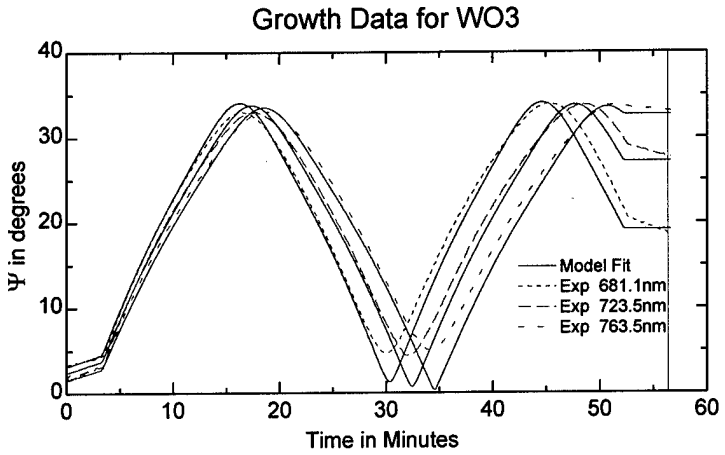

Figure 5: Insitu growth measurement of a cWO_3 film.

Ellipsometric optical studies were done in order to examine the optical properties of the constituent layers that make up a completed device. Optical constants varied from sample to sample, depending on preparation conditions. A detailed study was done on the effects of O_2 partial pressure on the optical properties of c-WO_{3-z}. The value of z has a large effect on the electrochromic properties of tungsten oxide. For the fits shown in the following figures a parameterized model was used. The model conisited of a sum of Gaussian and Lorentzian oscillators it was also necessary to add a Drude term to account for free carrier-like absorptions. The mathematical form of the model is:

$$\tilde{\varepsilon}(E) = \frac{A_1 B_1 E_1}{E_1^{\,2} - E^2 - iBE} + A_2 e^{-\left(\frac{E_2 - E_c}{B_2}\right)^2} + A_2 e^{-\left(\frac{E_2 + E_c}{B_2}\right)^2} + \frac{-A_3 B_3}{E^2 + iB_3 E}$$

Lorentzian Term Gaussian Term Drude Term

In Fitting the data with the above model A_1 corresponds to the strength of the Lorentzian Oscillator, B_1 is the broadening of the Lorentzian Oscillator, and E_1 is the center energy of the oscillator. A_2, B_2, and E_2 correspond to Strength, Broadening, and Center energy of the Gaussian Oscillator. The Drude term is similar to a Lorentzian Oscillator with a center energy of 0 eV, the A_3 and B_3 are the parameters used to describe the strength and Broadening of the Drude term. All of these parameters were specified to describe the data shown in figure 7-11.

The samples from the next figures were all been deposited on silicon substrates at 350°C. The only deposition condition varied was the O_2 partial pressure. The samples were reactively sputter deposited from a 5.08cm diameter target that was approximately 11.0cm from the substrate. The total pressure in the chamber during deposition was 15.0mTorr. Figure 6 shows the structure of the model used to fit the data.

The sample number corresponds to the O_2 partial pressure in the chamber during deposition.

Sample #	O_2 Partial Pressure
1	1 mTorr
2	2 mTorr
3	3 mTorr
4	4 mTorr

Paramaterized model c-WO_3	180 – 240nm
Native Silicon Oxide	1.88 nm
Silicon Substrate	1 mm

Figure 6: The structure of the model used to analyze the following data.

AS-DEPOSITED SAMPLE #1: 1mTorr O_2

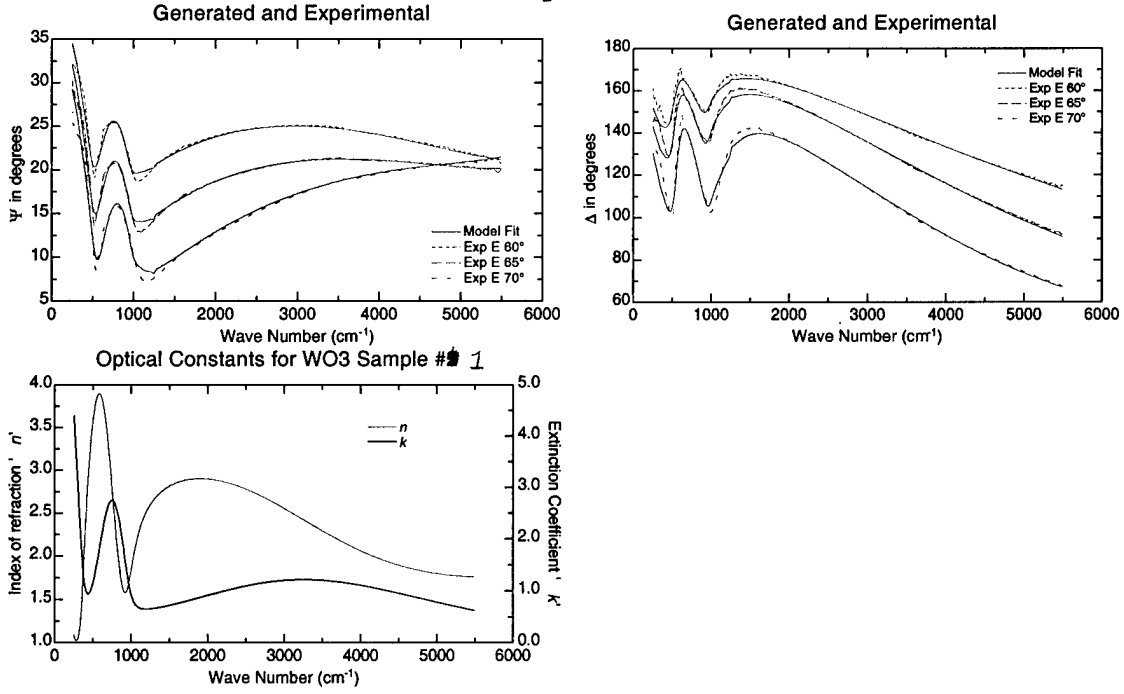

Figure 7: The ellipsometric data and corresponding fits for sample #1 a)ψ b)Δ c) The optical constants of c-WO_3 sample #1 extracted from the data fits.

AS-DEPOSITED SAMPLE #2: 2mTorr O_2

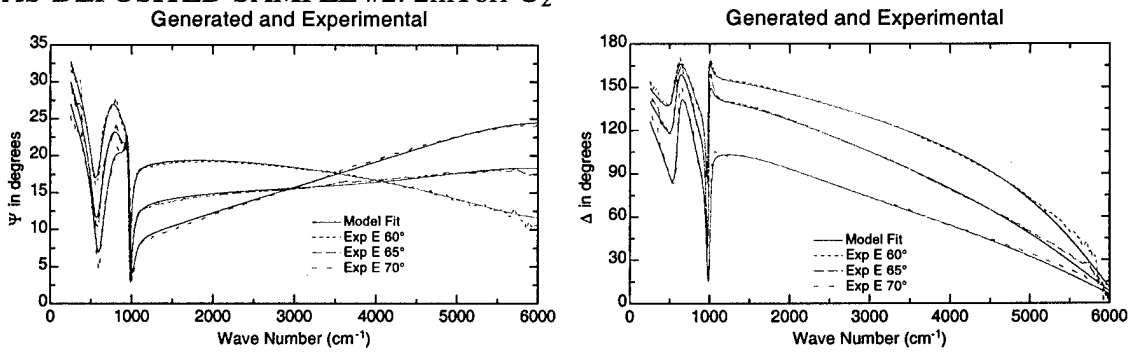

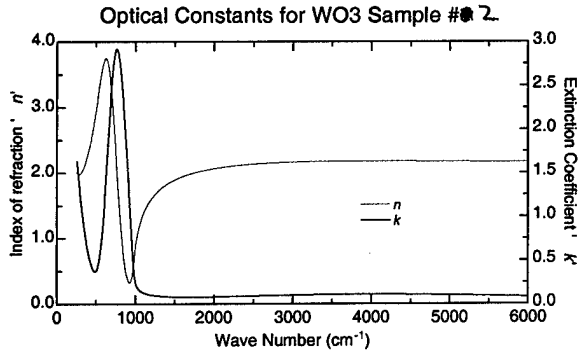

Figure 8: The ellipsometric data and corresponding fits for sample #2 a)ψ b)Δ c) The optical constants of c-WO_3 sample #2 extracted from the data fits.

AS-DEPOSITED SAMPLE #3: 3mTorr O_2

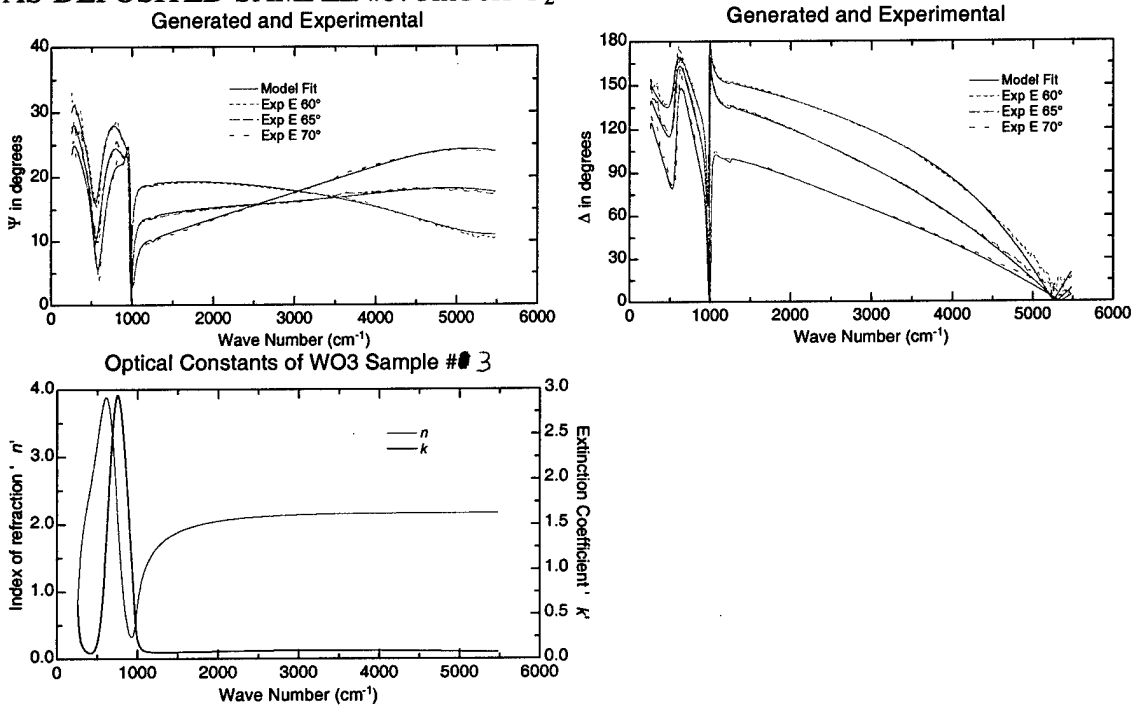

Figure 9: The ellipsometric data and corresponding fits for sample #3 a)ψ b)Δ c) The optical constants of c-WO_3 sample #3 extracted from the data fits.

AS-DEPOSITED SAMPLE #4: 4mTorr O_2

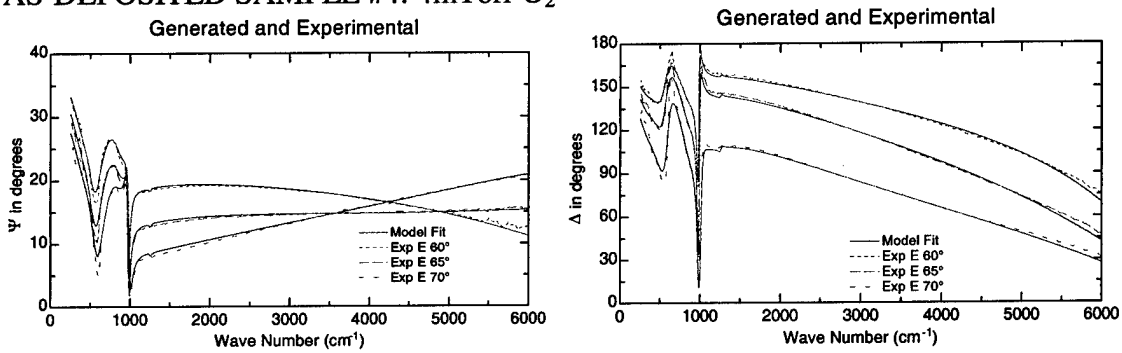

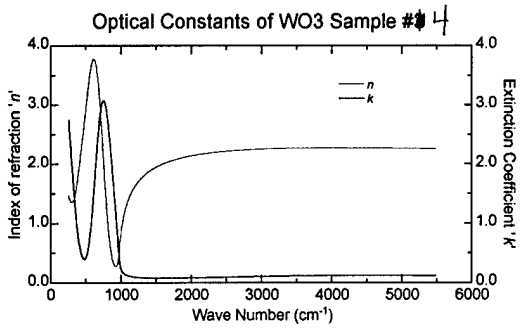

Figure 10: The ellipsometric data and corresponding fits for sample #4 a)ψ b)Δ c) The optical constants of c-WO_3 sample #4 extracted from the data fits.

Figure 11 summarizes the optical constants for the as-deposited films. All of the samples had virtually identical optical constants. Sample #4 had optical constants far different from those of the other three samples. The optical constants of the first three samples were very similar to the as-deposited optical constants after electrochemical intercalating and then deintercalating them. Sample #4's bleached optical constants were significantly different from the as-deposited state.

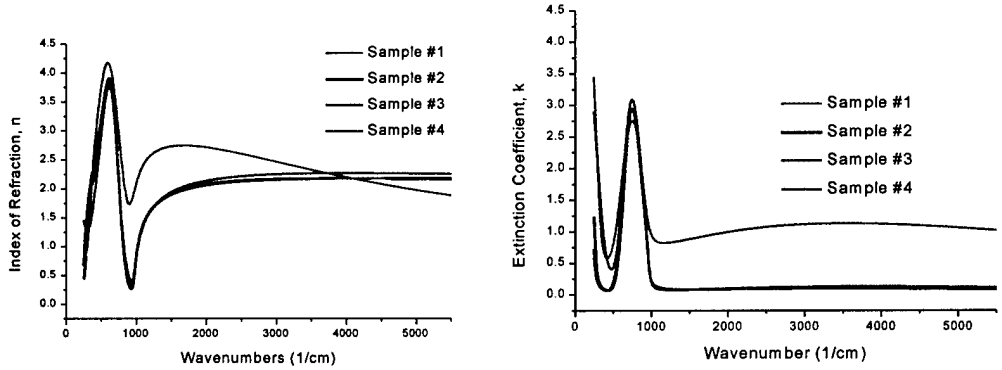

Figure 11: Summary of optical constants for samples #1-4 a) Index of Refraction, n b) Extinction Coefficient ,k

One important thing to note about the optical spectra of the all of these samples is the large absorption in the range of 600 to 1000 wavenumbers (10-16μm). This absorption is caused by the lattice structure of c-WO_3. The effects of this absorption are clearly seen in the coloring efficiency studies (Figure 4). It is in this same region of the spectra that the coloring efficiency of the films reaches a minimum. This minimum is due to the fact that the insertion of intercalant ions does not affect the major absorptions caused by the host lattice. For this reason the change in transmission per unit of charge inserted is very low in this region.

This brings up one of the drawbacks of the material. The room temperature blackbody spectra is peaked at the same point in the spectra as the lattice absorptions. For this reason maximum infrared (IR) emissivity modulation will be adversely affected in the most important part of the thermal IR spectral range.

Upon intercalating c-WO_3 films with Li^+ ions the optical properties change significantly. The effects of intercalation were studied on each of the above samples. Figures 13-16 show the ellipsometric data taken on the samples electrochemically intercalation. The model used to fit the data is similar, however another gaussian

oscillator was needed to describe a new absorption near 800cm^{-1}. It was also necessary to increase the strengths and broadenings of the previous absorption parameters. The mathematical form of the model for the intercalated c-WO_3 is as follows:

$$\tilde{\varepsilon}(E) = \frac{A_1 B_1 E_1}{E_1^{\,2} - E^2 - iBE} + A_2 e^{-\left(\frac{E_2 - E_c}{B_2}\right)^2} + A_2 e^{-\left(\frac{E_2 + E_c}{B_2}\right)^2} + A_4 e^{-\left(\frac{E_4 - E_c}{B_4}\right)^2} + A_4 e^{-\left(\frac{E_4 + E_c}{B_4}\right)^2} + \frac{-A_3 B_3}{E^2 + iB_3 E}$$

Lorentzian Term Gaussian Term #1 Gaussian Term #2 Drude Term

The difference between this model and the model used to fit the as-deposited data is the addition of the parameters A_4, B_4, and E_4. Corresponding to the Strength, Broadening, and Center energy of the new Gaussian absorption. Figure 12 shows the structure of the model used to fit the ellipsometric data shown in figures 13-16.

Paramaterized model for intercalated c-WO_3	180-240nm nm
Native Silicon Oxide	1.88 nm
Silicon Substrate	1 mm

Figure 12: Model structure for data shown in figures 13-16

INTERCALATED SAMPLE #1: 1mTorr O_2

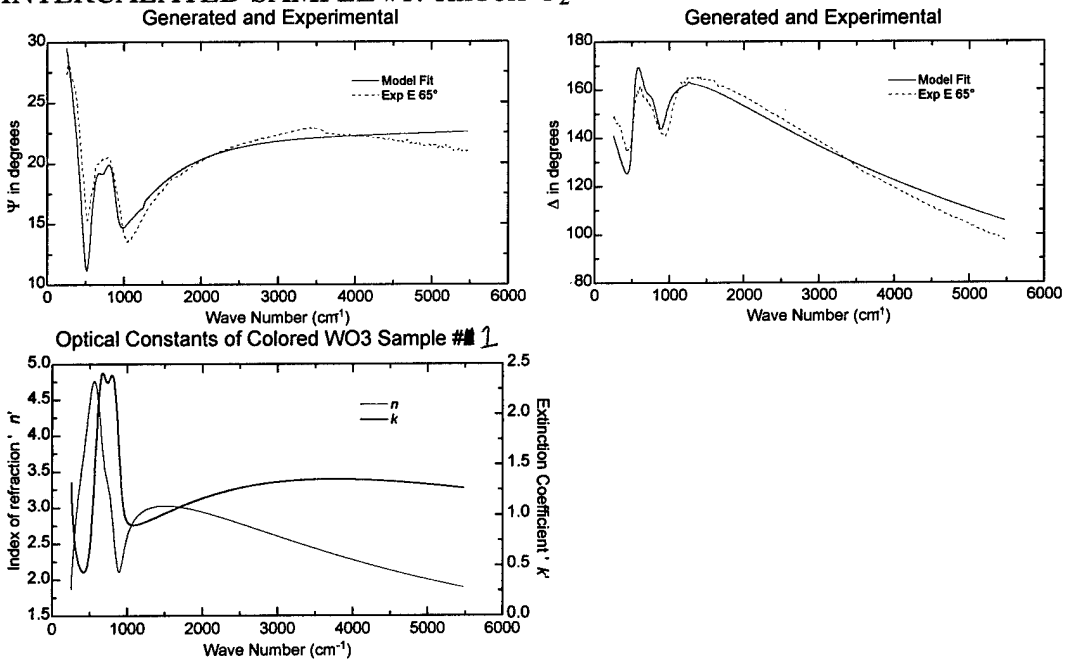

Figure 13: The ellipsometric data and corresponding fits for sample #1 after intercalation a)ψ b)Δ c) The optical constants of c-WO_3 sample #1 extracted from the data fits.

INTERCALATED SAMPLE #2: 2mTorr O_2

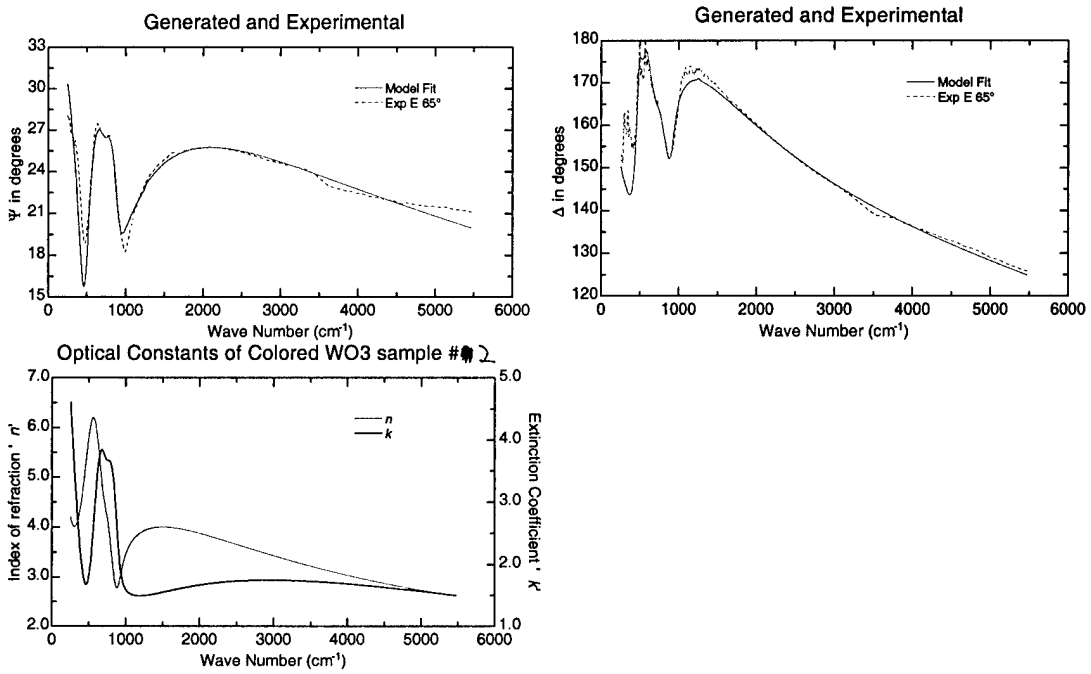

Figure 14: The ellipsometric data and corresponding fits for sample #2 after intercalation a)ψ b)Δ c) The optical constants of c-WO_3 sample #2 extracted from the data fits.

INTERCALATED SAMPLE #3: 3mTorr O_2

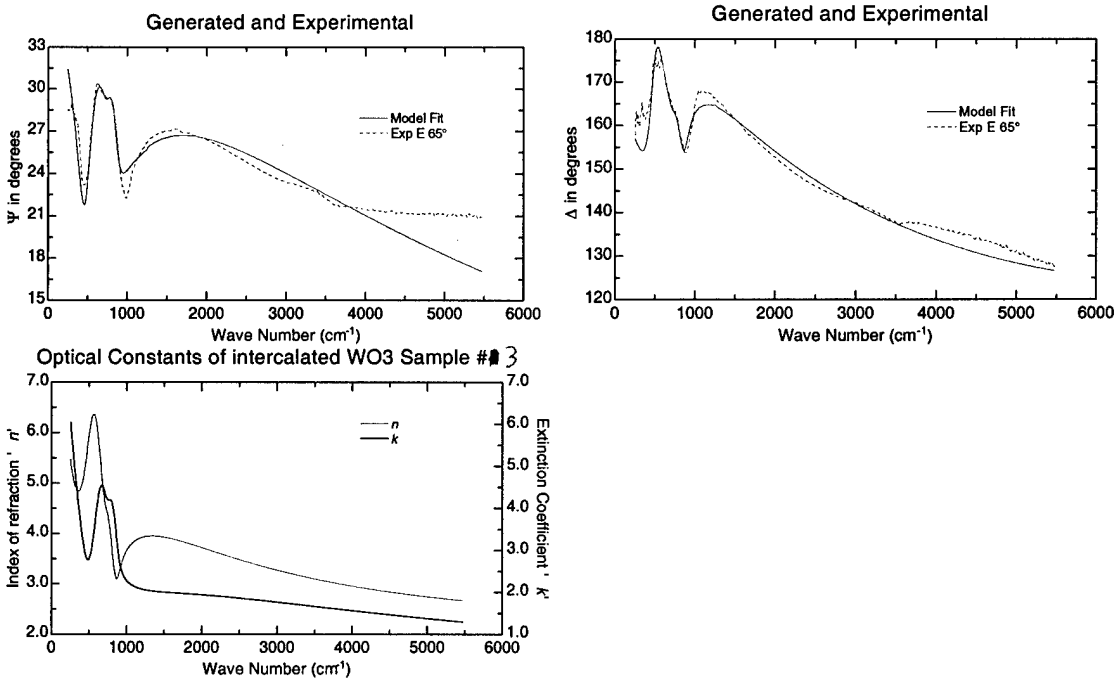

Figure 15: The ellipsometric data and corresponding fits for sample #3 after intercalation a)ψ b)Δ c) The optical constants of c-WO_3 sample #3 extracted from the data fits.

INTERCALATED SAMPLE #4 4mTorr O_2

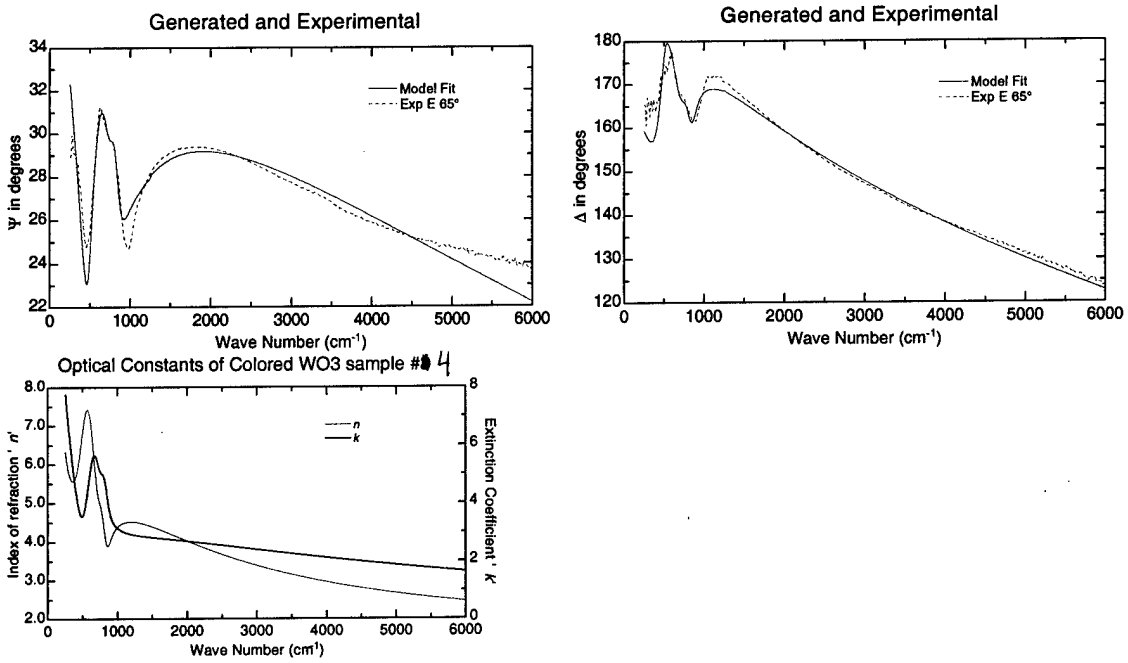

Figure 16: The ellipsometric data and corresponding fits for sample #4 after intercalation a)ψ b)Δ c) The optical constants of c-WO_3 sample #4 extracted from the data fits.

Figure 17 summarizes the optical constants for each of the above samples. Both the index of refraction and extinction coefficient increase across the entire range of the spectrum. There is also a new absorption shown in the extinction coefficient at approximately 900 wavenumbers. This shoulder is not seen in the film before intercalation. In the shorter wavelength region both the index and the extinction coefficient are significantly different from the optical constants of as-deposited films.

An increase in O_2 partial pressure leads to a higher absorption across most of the spectral region. However, sample #4, the sample deposited with the highest O_2 partial pressure, did not return to the as-deposited state upon deintercalation. This information allowed us to optimize the O_2 flow rate into the chamber in order to obtain films that were the most durable.

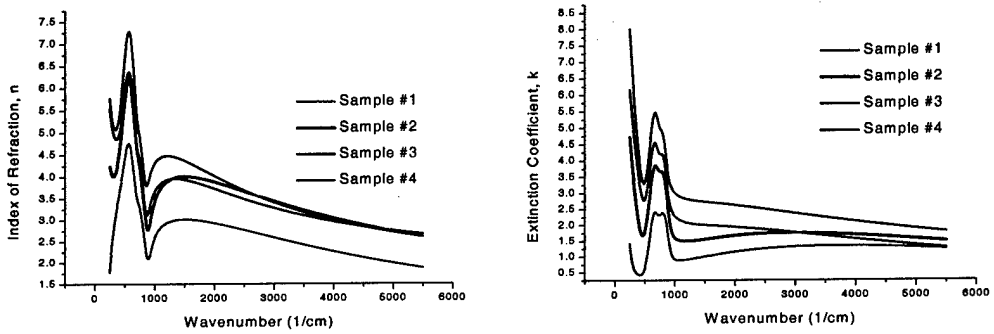

Figure 17: Summary and comparison of the optical constants for samples #1-4 after electrochemical intercalation.

B. Amorphous Tungsten Oxide

Amorphous Tungsten Oxide (a-WO_3) is one of the most frequently investigated electrochromic materials. Thorough studies have been made on the material for applications requiring variable optical properties in the visible region of the spectrum.

The role a-WO_3 plays in our IR devices is as a charge storage layer. When the c-WO_3 top layer is bleached (that is, no mobile ions are intercalated into it), the mobile ions will be stored in the a-WO_3 layer.

This would not be a feasible material choice if we were developing a device for visible operation, because the device would always have one layer that is in its low transmission state.

Due to the fact that we are not concerned with visible operation this material choice is ideal for several reasons. It has an ion capacity similar to the c-WO_3 and the films can have similar thickness. The fabrication of a device is also greatly simplified because the only difference between the deposition conditions of the c-WO_3 and the a-WO_3 is the temperature; all other processing conditions are the same. This eliminates one pump down step, decreasing the time of making a device by one day. The material is also compatible with the other layers of the device.

There has been a lot of attention paid to a-WO_3, and a vast body of work has been devoted to its study. The durability of devices for visible operation has improved dramatically in the last decade. This indicates that the material is a good choice for utilization in devices with long lifetime requirements.

For an IR modulating device the amorphous form of the oxide is not a good choice for the optical switching layer. Its ability to modulate infrared frequencies is hampered by a polaron absorption in the near-IR. The IR optical properties of a-WO_3 do not change as much as the IR characteristics of c-WO_3. Figure 18 shows ellipsometric data taken on an amorphous film deposited on an optically thick metallic layer before and after electrochemical intercalation with Li^+. The models used to fit these data were similar to that for the c-WO_3. For the measurement done on the as-deposited sample 3 Lorentzian oscillators were used. For the intercalated sample only 2 oscillaters were necessary because the absorption near 370cm^{-1} was not seen.

The model for the as-deposited model had the following form:

$$\tilde{\varepsilon}(E) = \varepsilon_\infty \sum_{n=1}^{3} \frac{E_{nLO}^2 - E^2 - iB_{nLO}E}{E_{nTO}^2 - E^2 - iB_{nTO}E}$$

This is a different form of the Lorentzian oscillator equation, and the parameters used in fitting were E_{nLO}, B_{nLO}, E_{nTO}, B_{nTO} corresponding to the center energy, broadening, and strength of the absorptions.

For the intercalated model the same form was used however there were only two oscillators (n=1,2) instead of three.

Figure 19 shows the optical constants that had been extracted from the ellipsometric data. From this figure it is evident that the change in optical properties upon intercalation is not as large with a-WO_3 as it is with c-WO_3.

a)

Paramaterized model of a-WO_3	342.31 nm
Optically thick Tungsten metal	25 nm
Glass Substrate	1 mm

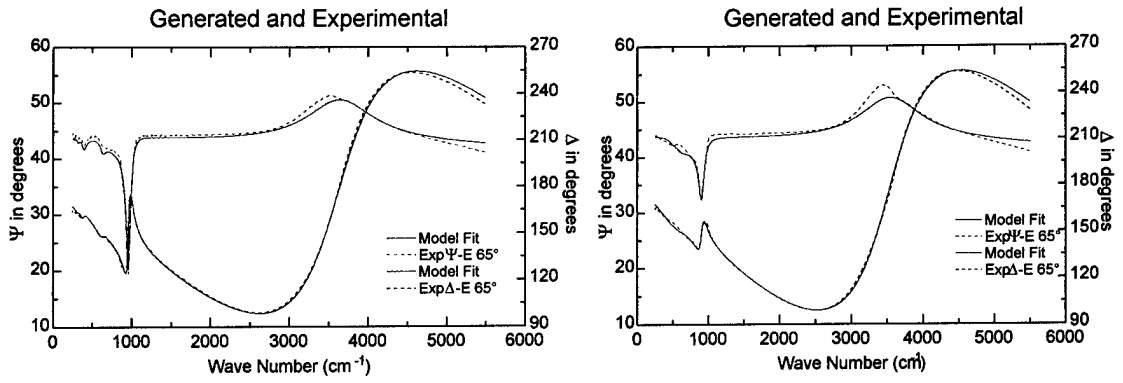

Figure 18: Ellipsometric ψ, and Δ spectra of a-WO_3 , and fit of the a)parameterized optical model used to analyze the data. A)Before any electrochemical processing had been done. B) After the film had been electrochemically intercalated.

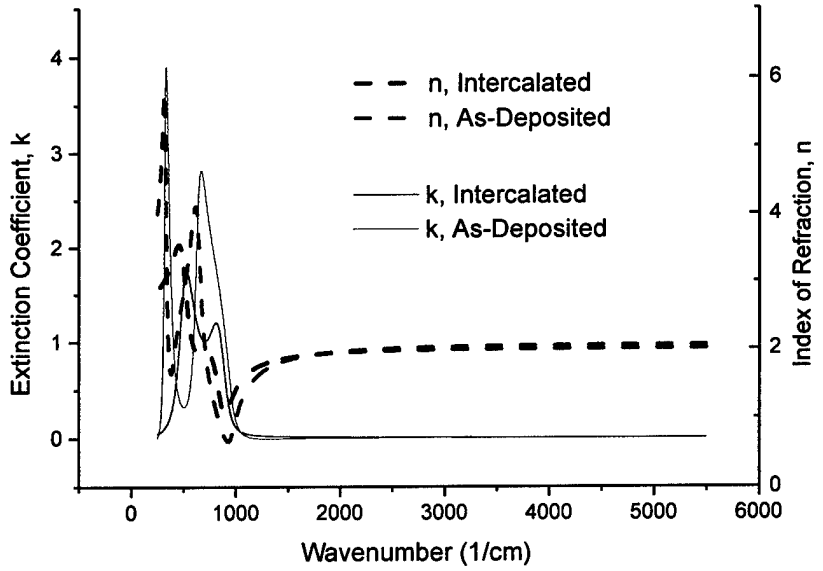

Figure 19: Comparison of optical properties between intercalated and as deposited states of a-WO_3.

In order to study the nonuniformity in deposition thicknesses an ellipsometric X-Y profiling measurement was done. A sample was measured in several different places. This was an effective way to develop a 'topographical' map. The thickness nonuniformity is caused by the geometric relation between the sputter gun and the substrate. The results show that the films have a nonuniformity of less than 5% from the center of the substrate to the edge. Figure 20 shows the results of this study done on an a-WO_3 film.

Devices were commonly made with dimensions of about 2cm by 2 cm. Within this size the material was approximately ±2% uniform.

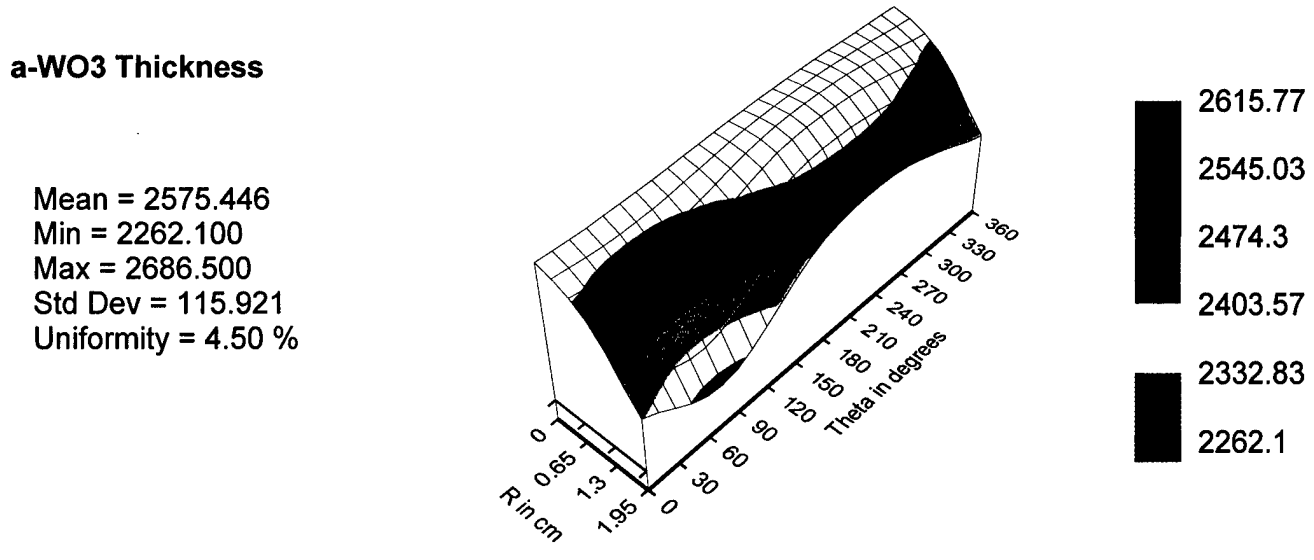

Figure 20: Nonuniformity ellipsometric mapping of a-WO_3.

C. Nickel Oxide

Nickel Oxide is a well established material utilized in battery technology. It is able to reversibly incorporate Li^+ and H^+ into its lattice. Some success in utilizing NiO as an electrochromic charge storage layer has also been realized. In this capacity the material acts as a complimentary electrochromic layer to WO_3. When mobile ions are intercalated into WO_3 films they become dark, the situation is reversed in the case of Nickel Oxide. When mobile ions are intercalated into NiO they film become clear. This allows maximum transmission in visible devices.

Our early work took advantage of this transparency switching property to make devices using polymeric ion conductors. The polymer based devices required an electrochromic film that was transparent to UV light so that the ion conducting polymer could be cured after it had been placed between the two electrochromic half devices (this process will be described in detail in section III). We also used NiO in later solid-state device trials in order to measure visible performance of proposed devices.

There are several reasons this material was changed in favor of a-WO_3 for our final solid-state devices. The voltage cycling of the devices seemed to degrade the films for both H^+ and Li^+ intercalated devices. It is still not clear what causes the degradation.

In devices that utilized polymers for ion conductors some reaction took place at the nickel surface causing the formation of what appeared to be crystals. We could not separate the two halves of the device in order to analyze the products of the reaction and we cannot say with certainty what caused this breakdown.

Something similar also happened when we used NiO in solid-state devices. After several cycles the films appeared to delaminate from the substrate. The density of what appeared to be cracks in the film increased as the switching voltage was increased.

As with the previous films ellipsometric analysis was used to determine the infrared optical properties of NiO in both the intercalated and unintercalated states.
Figure 21 shows the ellipsometric data from a nickel oxide sample that had been deposited on an ITO coated glass slide.

These data were fit with a lorentz oscillator and a drude term. The model had the following mathematical form:

$$\tilde{\varepsilon}(E) = \frac{A_1 B_1 E_1}{E_1^{\,2} - E^2 - iBE} + \frac{-A_2 B_2}{E^2 + iB_2 E}$$

Lorentzian term Drude Term

Amplitudes, center energies, and broadenings were specified in order to obtain the fits shown in Figure 21. Figure 21b shows the optical constants extracted from this model.

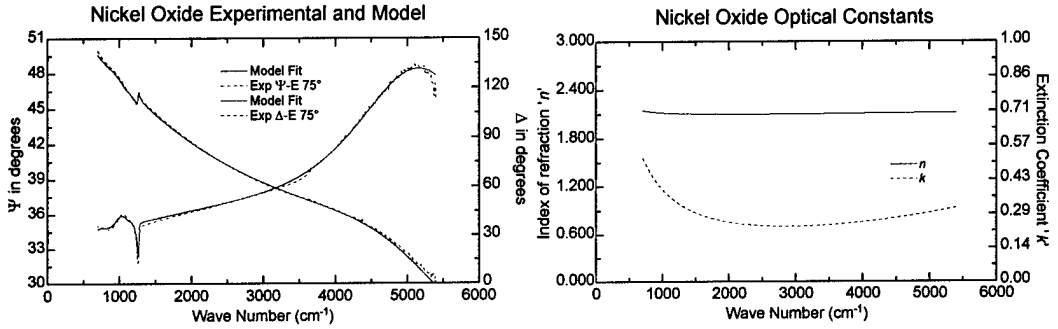

Figure 21: a)Ellipsometric data taken on a thin film of Nickel oxide on an ITO coated glass slide. Also shown is the fit of the optical model used to analyze the film. b) The optical constants of Nickel oxide extracted from the model.

The effect of intercalation on the IR reflectivity of nickel oxide films was studied. Figure 22 shows the results of taking reflection measurements on a sample before any processing had been done, and the measurement after the sample had been intercalated with Li^+.

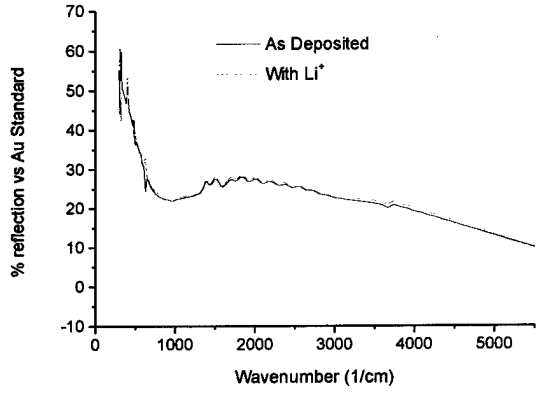

Figure 22: Comparison of reflectivity of as-deposited nickel oxide and Li^+ intercalated nickel oxide.

As shown above the reflection data from single films of nickel oxide were not significantly affected by intercalating the films with a mobile ion species. Also in the modeling of devices the optical constants of the nickel oxide film didn't drastically effect the theoretical reflection. For this reason the optical constants obtained from an as-deposited film were used in predicting the performance of devices that utilized nickel oxide as a charge storage material.

D. Tantalum Oxide

Tantalum Oxide Ta_2O_5 is utilized as an ion conducting material. This was a layer used in the fabrication of monolithic, all vacuum deposited device structures. This material is one of the more critical layers in the device operation. Although its effect on the reflectivity of the completed device is not as great as that due to c-WO_3, it has a significant effect on the ability of the device to reversibly change its emittance states, and on the memory of the device.

Ta_2O_5 is a good electrical insulator. However because the porosity of the films we have been able to make is high, the electrical conductivity is high. In some cases this is detrimental as far as device operation is concerned because it requires a much higher driving voltage to shuttle the ions across the layer to switch the device. This higher driving voltage decreases the lifetime of the device.

In other cases the electrical conductivity is so high that ions will not move from the electrochromic layer to the charge storage layer and the device will not perform at all.

In order to try to minimize the problem of electrical conductivity it is necessary to maximize the density of the thin films. In order to gauge the effect of deposition parameters on the density of the films AFM, and UV-VIS ellipsometric data were taken on films that had been deposited under different conditions. In order to fit the ellipsometric data it was assumed that all four samples had the same optical constants (obtained from published data) and the only difference between them was the porosity of the samples. This was done by utilizing an effective medium approximation (EMA), to model the data. Figure 23 shows the results of the AFM measurement and Figure 24 shows the fits to the ellipsometric data with the final value of porosity for each of the corresponding samples.

These data show good agreement between the two measurement techniques and helped us to determine the deposition conditions that would provide for films of the highest density.

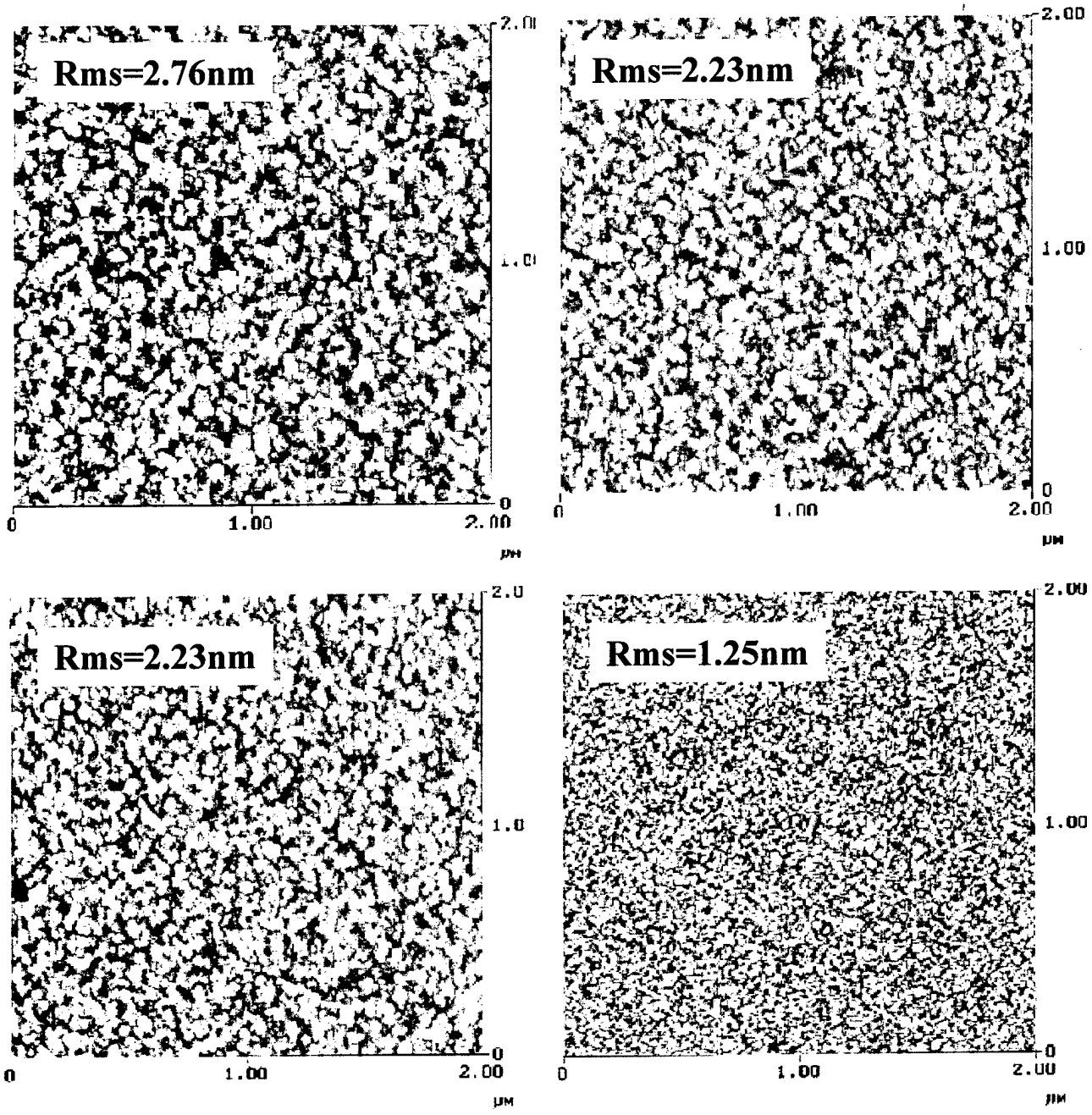

Figure 23: Results of AFM measurements done on four samples of Tantalum Oxide deposited at various deposition conditions. An increase in O_2 flow rate and Temperature gave the lowest RMS values.

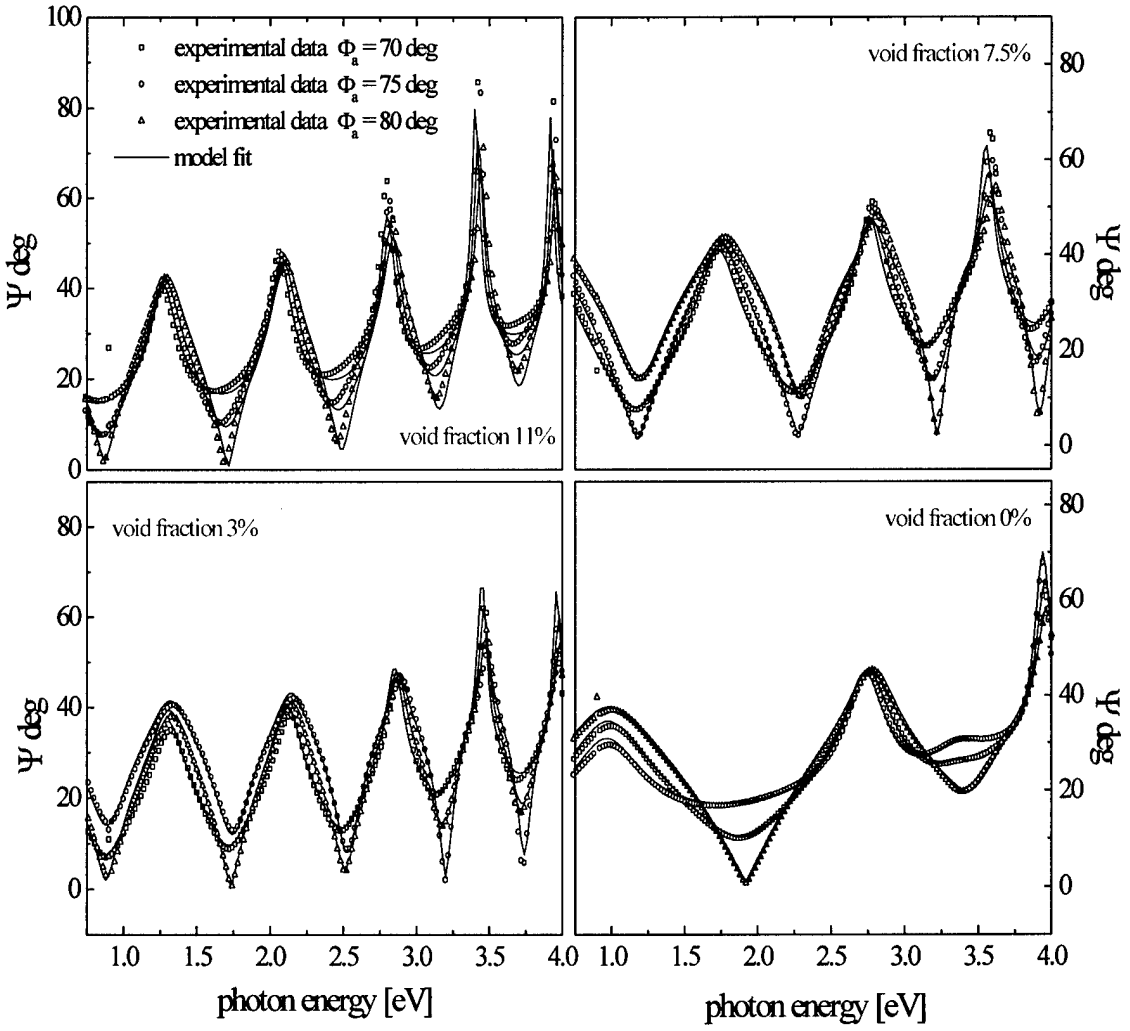

Figure 24: The ellipsometric data fits for the same samples as shown in the AFM results. The highest void fraction corresponds to the roughest of the films while the lowest void fraction corresponds to the smoothest film.

Much work was done on this material in order to better understand the structural properties so that good electrically insulating films can be deposited. Extensive optical analysis has been done to meet this end. In the technical publications section is a detailed paper (submitted January 2000 to the Journal of Applied Physics for publication) documenting our results.

As with the other material this film was studied as a single film on a substrate apart from device applications. The IR data fit and the corresponding optical constants for the smoothest sample (lowest void fraction) is shown in Figure 25.

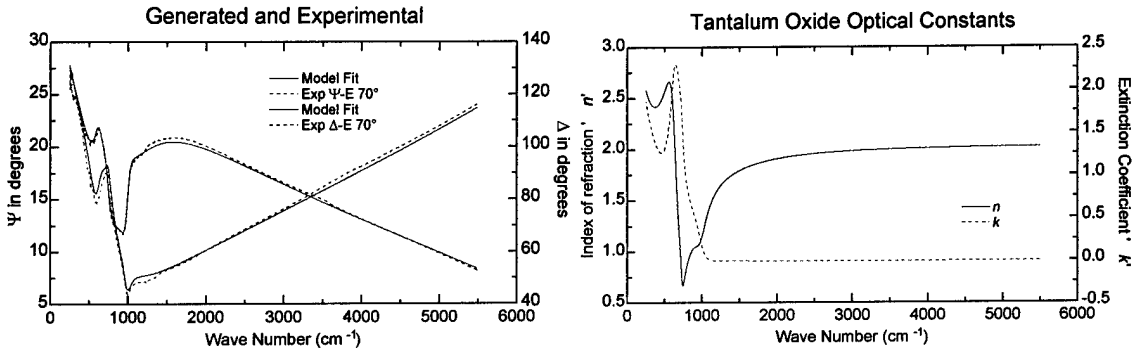

Figure 25: Results of IR ellipsometric analysis on the Tantalum Oxide sample with the highest density a) Ellipsometric Ψ, and Δ spectra and the fit of the optical model used to analyze the film. b) The optical constants of the film extracted from the model.

E. AMPS/DMA Polymeric Ion conductor.

This material was used for the same purposes as Tantalum Oxide in several early devices. It provided a path for the mobile ions to move from the electrochromic layer to the charge storage layer. It also provided electrical insulation between layers so that complete electrochromic devices would possess a 'memory'.

The material and the method of making it was obtained from U.S. Patent No. 5,520,851 regarding electrochromic devices. Details of the chemistry can be found in the patent, which describes use of the polymer as a H^+ conducting material. By adding $LiClO_4$ the polymer was able to conduct Li^+ as well. AMPS/DMA is relatively simple to produce and provides much better electrical insulation than Tantalum Oxide. It also allowed fabrication of devices that worked well enough to provide a baseline performance index with which to compare monolithic devices (devices made by all-vacuum processes).

Like all other materials, it was necessary to obtain the optical constants of the polymer in order to model our devices. This was done by utilizing an attenuated total reflection (ATR) technique. A ZnSe, IR transparent prism was coated with the polymer and then an ellipsometric measurement was taken. This allowed the polymer to be treated as an optically thick material and the optical constants could be extracted directly from the ellipsometric data. Figure 26 shows the results of the measurement and the optical constants obtained.

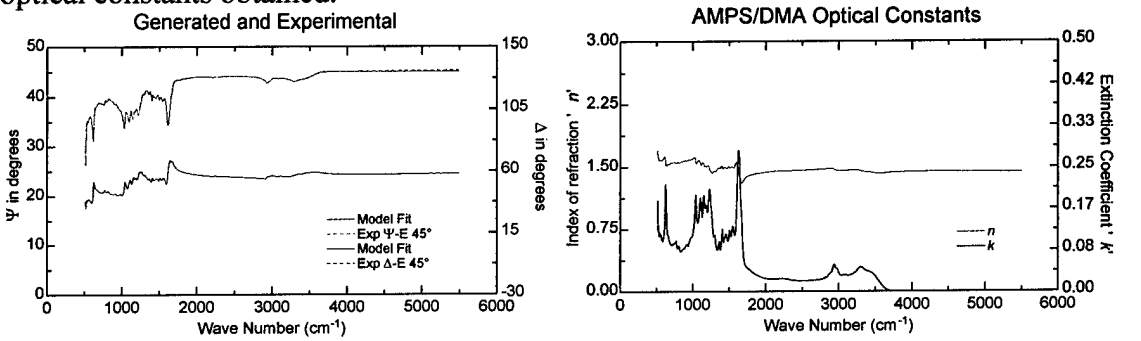

Figure 26: a) Ellipsometric ATR data taken on AMPS/DMA. Also shown is the fit of the data. b) The optical constants of AMPS/DMA extracted from the ellipsometric data.

There are several problems associated with Polymeric ion conductors. The most important drawback is the inability to fabricate an all-vacuum deposited monolithic

device utilizing a liquid polymer. The second drawback is the durability of the material under conditions where long switching lifetimes are desired. In our early devices the polymer contributed to breakdown in device operation by reacting adversely with either the other films that make up the device, or the mobile ions. Over several switching cycles there appeared to be some crystallization of the salts used to make the polymer ion conducting.

It is not known whether the polymer is reacting with the electrochromic materials or with the mobile ions. The same failure was seen in both H^+ and Li^+ devices. The products of this side reaction are not known because it is impossible to separate the devices and perform any analysis on the polymer. After this reaction has taken place the devices failed to switch from one state to the other.

Another problem with the material is that it has several optical absorptions in the IR region where the devices should operate. This is shown by the high value of the extinction coefficient between 2000 and 350 cm^{-1} in Figure 26b. Due to the fact that this layer is the thickest layer in the device (typically 25μm) these absorptions dramatically decrease the IR device performance.

F. Low dopant concentration silicon substrates.

Silicon wafers with a low dopant concentration (resistivity of 3-5 ohm-cm) were used as substrates for many of the devices. These wafers are conductive enough to use as conducting layers, and transparent enough to make IR transmission or reflection studies.

There were several benefits of using these substrates. They have low cost, and we are able to purchase them from any silicon vendor, in a large volume if necessary. For device operation, they are good IR transparent substrates over the spectral range of 5500cm^{-1} to 300 cm^{-1}. Figure 27 shows a transmission measurement taken on one of the Silicon wafers, it is evident that roughly 50% of the incident radiation passes completely through the wafer.

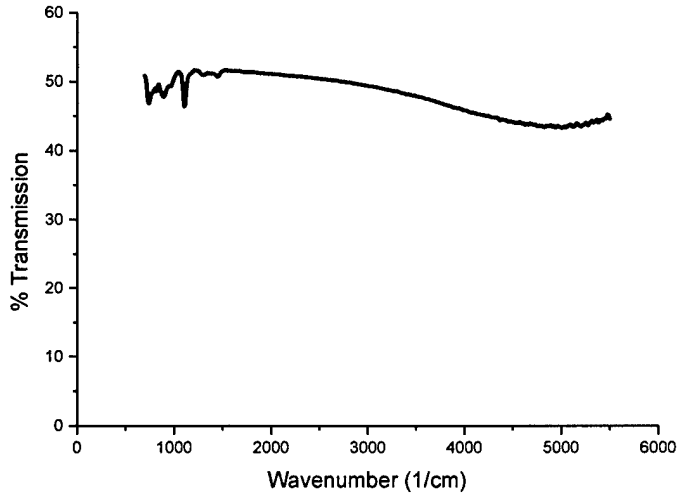

Figure 27: The transmission measurement of IR radiation through the high resistivity Si substrates.

Another benefit of using silicon as a substrate is that the optical properties over the spectral range that we are interested in are well known. This allows us to focus our

studies on the thin films deposited on silicon, and to separate substrate effects from optical characteristics of the thin films under study. Figure 28b shows the IR ellipsometric data on a high resistivity Si wafer. The IR optical properties of Silicon are heavily dependent on the concentration of impurities. For this reason an ellipsometric measurement was made on a wafer similar to the ones used for devices. Figure 28c shows the difference between the optical model and the experimental data obtained during the measurement.

The optical model was a simple drude model that describes the effects of free carriers in the silicon. The model has the mathematical form of:

$$\hat{\varepsilon}(E) = \varepsilon_{1\infty} - \frac{A}{E^2 + iBE} \text{ where } A = \frac{\hbar^2}{\varepsilon_0 \rho \tau} \qquad B = \frac{\hbar}{\tau}$$

ρ is the resistivity of the material and τ is the mean scattering time between collisions for the carriers. In modeling this sample we fit for the $\varepsilon_{1\infty}$,ρ, and τ parameters.

There is good agreement between calculated optical properties and measured data. The results of this experiment are utilized in modeling devices.

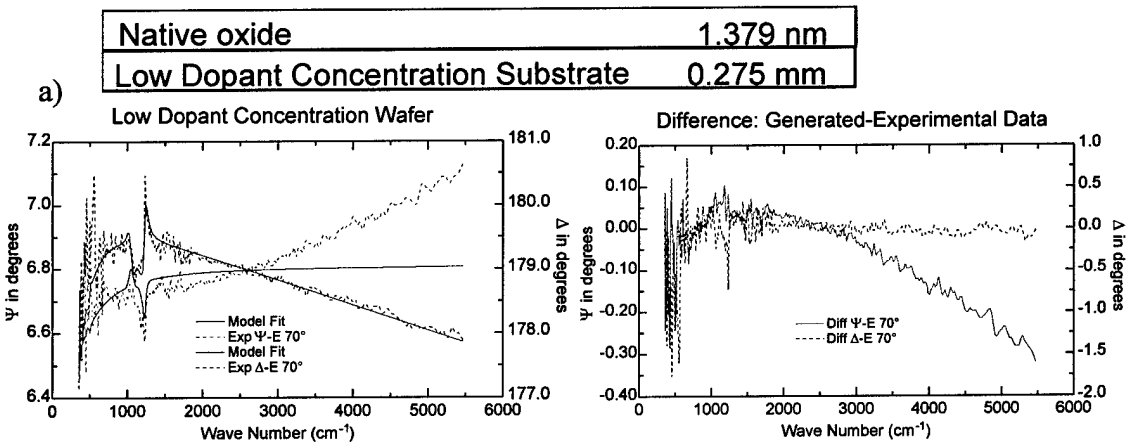

Figure 28: a) The model used to fit the data b) Ellipsometric Ψ and Δ data measured from a high resistivity Si wafer. This figure also shows fit of the modeling. c) The difference between the model generated data and the experimental data.

There is an important drawbacks to using silicon wafers in IR electrochromic devices. The first is that silicon is thick. At 275μm the radiation has to go through a lot of material and any absorptions at all, however slight, will effect the measured device performance.

G. Indium Oxide doped with Tin Oxide (ITO)

ITO is frequently utilized as a transparent electrical conducting material in many applications. In our case we used it in polymer based devices and also in some monolithic devices. It provides the electrons a path to the electrochromic films.

The transparency of ITO served two purposes. In the polymer devices we needed a transparent conductor so light could shined on the uncured polymer. In solid-state device development the transparency allowed transmission measurements to be made with a UV/VIS spectrophotometer. It also allowed us to qualitatively determine whether

or not the monolithic solid-state devices were switching between the colored and bleached states.

The other benefit of using ITO as a transparent conductor is that it is readily sputter deposited, and varying the deposition temperatures easily enhanced the electrical conductivity.

In order to model devices that used ITO as an electrical conductor we again did ellipsometric studies on the material. Figure 21a shows the ellipsometric data and the fit of the optical model used to analyze it. The model used was exactly the same as the model used to determine the optical properties of the Silicon substrate above. The values of the parameters were the only difference between the models.

The sample was deposited on a quartz disk at room temperature. Figure 21b shows the optical constants extracted from the model. These optical constants were used in modeling complete devices.

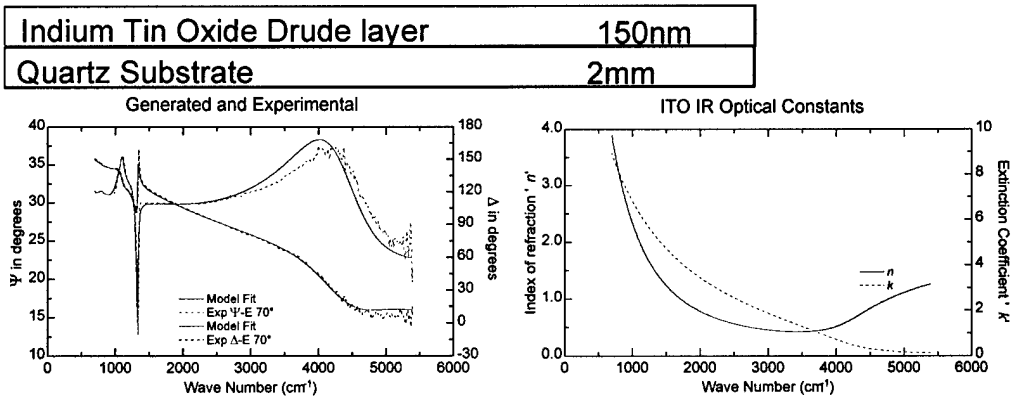

Figure 29: a) The structure of the model used to fit the data b) Ellipsometric Ψ, and Δ data and the fit of the model B) The IR optical constants of ITO films deposited at room temperature.

H. Other Materials

Lithium Aluminum Floride (LiAlF) was also investigated as a ion conductor. A search of the literature suggested that this material could be a good possible fast-ion conductor while maintaining good electrical isolation between the two electrochromic layers.

The difficulty with utilizing (LiAlF) is that it is a ceramic and very difficult to sputter deposit. Deposition times of more than an hour made at high power produced films that were approximately 100nm thick. Films this thin do not provide enough material to electrically insulate the electrochromic films from one another because there is a high density of pinhole shorts.

The mobility of Li^+ through sputter deposited LiAlF was prohibitively low. After depositing the material on a film of cWO_3 it was not possible to induce a color change by electrochemical intercalation.

Aluminum Oxide(AlO) was also reported in the literature to be an ion conductor, and several attempts at sputter deposition from an Aluminum Oxide target were made. It was not possible to obtain films on the glass or silicon substrates even under maximum power and various deposition environments.

Vanadium Oxide was investigated as a charge storage material. Vanadium Oxide has a high ion capacity, and a polymeric device was made with this material by replacing nickel oxide. It is fairly transparent in the visible and it allowed for curing of the polymeric ion conductor. Like nickel oxide it is often utilized in battery technology.

The number of Vanadium and Oxygen metallurgical phases is very high, and it is difficult to ascertain with certainty the phase and stochiometry of our vanadium oxide. These films were likely of mixed phases.

Unfortunately, unlike nickel oxide the vanadium oxide does not adhere well to either ITO coated glass or silicon substrates. Deposition conditions were found that did make films which would adhere, however these peeled off the substrates after rinsing with deionized water. In order to make a device with vanadium oxide storage layer the film was not rinsed after electrochemical intercalation.

PART III: POLYMERIC ION CONDUCTING DEVICES

A) INTRODUCTION

The electrochromic devices made during this contract fall into two broad general categories. The first category is made up of devices that use two substrates and are laminated together by a polymer that provides the ion-conducting layer. The second category is a monolithic structure consisting of films that were all sputter deposited.

In order to construct the first type of devices two different substrates were used. The first was either a glass slide, or a quartz disk. The second substrate was a silicon wafer with an impurity concentration low enough to allow good IR transparency, but high enough to allow good electrical conductivity (See Part II: Materials).

In order to determine the portion of the blackbody that our measurements encompassed the following equations were used:

$$M(\sigma,T) = 2\pi h c \sigma^3 \times \frac{1}{e^{\left(hc\sigma/kT\right)} - 1} \quad (1)$$

$$\text{Percent of BlackBody Covered} = \frac{\int_{\sigma 1}^{\sigma 2} M(\sigma,T)}{\int_{0}^{6000 cm^{-1}} M(\sigma,T)} \quad (2)$$

Where $\sigma 1$ and $\sigma 2$ define the lower and upper limit of the spectral region that were measured. The blackbody emissivity spectrum extends out to infinite wavenumbers, it approaches the limit of 0 (W/cm^2 wavenumbers) well before 6000 cm^{-1}. The integral in the denominator of equation 2 makes the assumption that 100% of the blackbody is contained between the limits of $0cm^{-1}$and $6000cm^{-1}$.

The results of the emissivity integration are shown in the figures detailing the performance of each device. These results are summarized by the tables at the end of sections III and IV.

B) FABRICATION AND STRUCTURE

These devices were made in two halves, on on glass, one on a polished Si wafer. First a film of ITO was sputter deposited on to a glass slide. This ITO provided one of the electrical contacts. Over the ITO a nickel oxide film was deposited and used as a charge storage layer. Silicon was used as a second substrate for deposition of polycrystalline WO_3.

After the thin films were deposited the cWO_3 was electrochemically intercalated in either 1.0M H_2SO_4 or 1.0M $LiClO_4$ solutions, the former for H^+ the latter for Li^+. The electrochemical cell that was used for the color bleach cycles was a three electrode cell with a saturated calomel reference electrode and a platinum foil as the working electrode. The film being cycled was the working electrode and it was placed about 3 cm from the

other two electrodes. The cWO_3 half of the device was cycled through several color bleach cycles with voltages of –1.0V and +1.0V respectively and then removed from the electrochemical cell in the intercalated state. The same procedure was used to prepare the nickel oxide half of the device cycling the voltages between –0.375V and +0.650V, but it was removed from the electrochemical cell in the unintercalated state.

Next a few drops of polymer were placed on the cWO_3 half of the device, and finally the nickel oxide side was "sandwiched" to the top of this. The polymer with a UV light source shined through the nickel oxide. The device structure is shown in Figure 2. Electrical contact was made to the device with alligator clips. Figure 2 also shows how a reflectance measurement was taken and the location of contacts with the external power source.

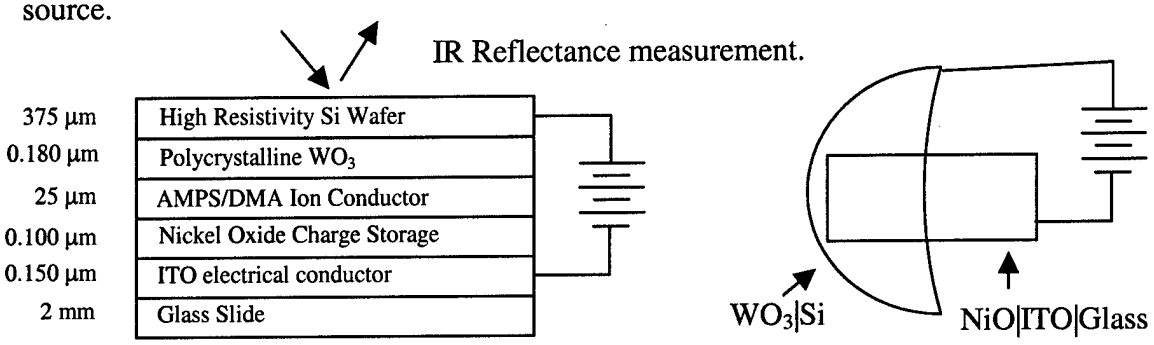

Figure 2: Structure of polymeric ion conducting device, including the location of the electrical contacts to the external source and the method in which the reflectance measurement was taken.

These devices stopped showing color changes from one cycle to the next after 3 or 4 cycles, presumably due to polymer electrolyte degradation. The cause of the degradation is unknown because the devices could not be separated after the laminating polymer was cured. There was evidence to suggest that the polymer had undergone some type of side reaction. This reaction caused formation of what appeared to be crystallites in the polymer film. After formation of crystallites and the inability to insert any charge into the device no further measurements were taken.

The following figures show the results of several devicesbased on polymer ion conductors: At the end of this section a summary of the emissivity modulation of each of these devices is tabulated, indexed by the heading of each performance figure.

C) PERFORMANCE OF POLYMER BASED DEVICES

DEVICES UTILIZING H^+ IONS

I) Device #1 (H^+ ions)

For this device 95% of the blackbody region was covered in the measurement.

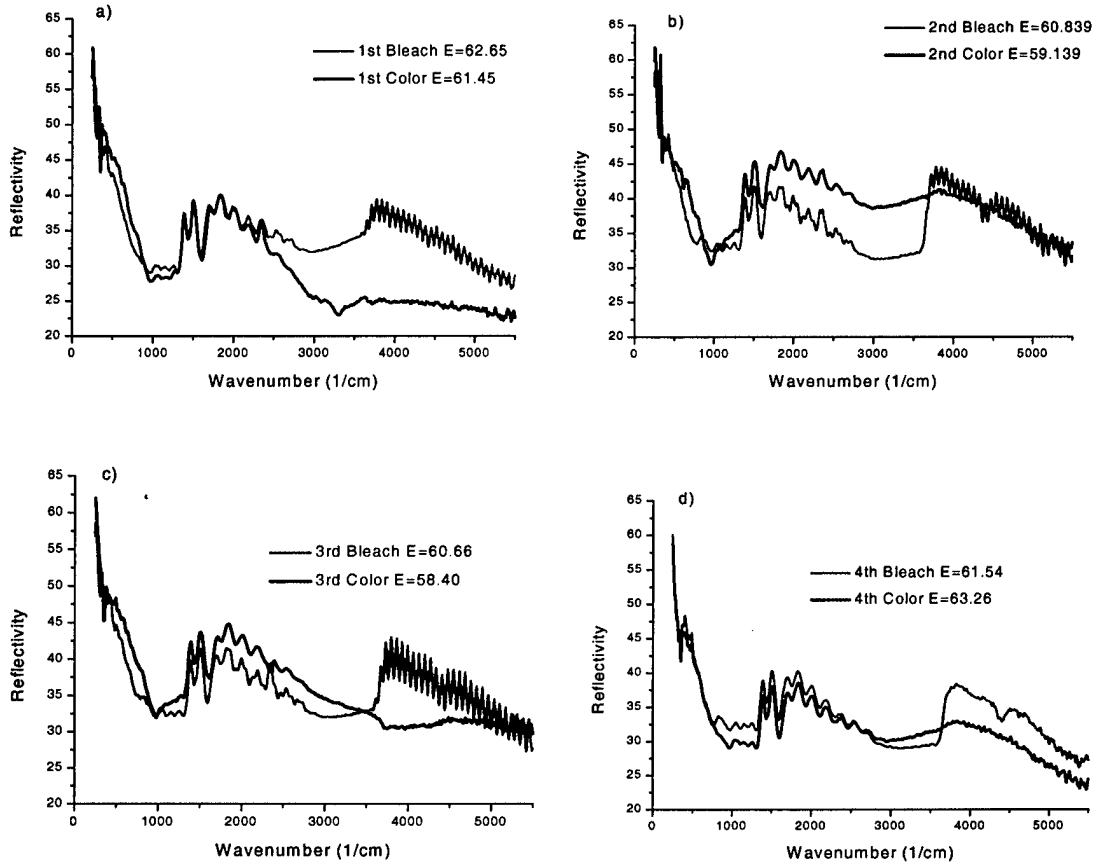

Figure 3: The measured reflectance of Device #1 (H^+ions) the first device with ▬ the top c-WO_3 unintercalated (bleached) and ▬ with the top c-WO_3 intercalated (colored). a) First Cycle b) Second Cycle c) Third Cycle d) Fourth Cycle.

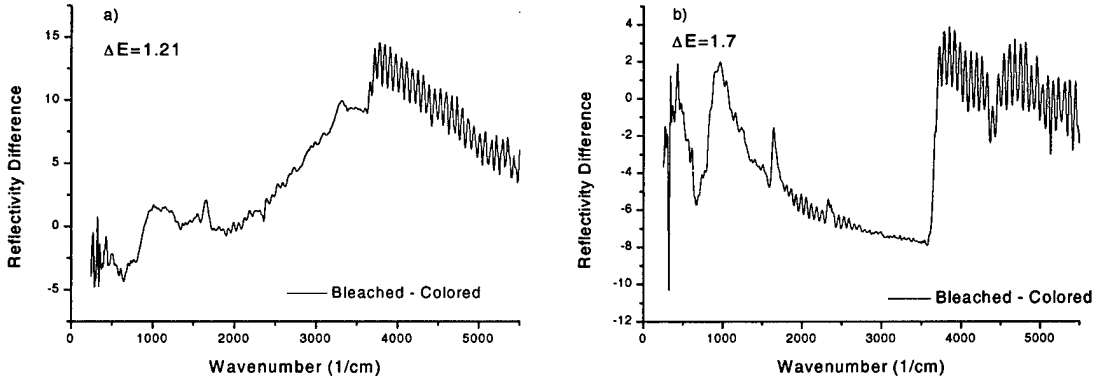

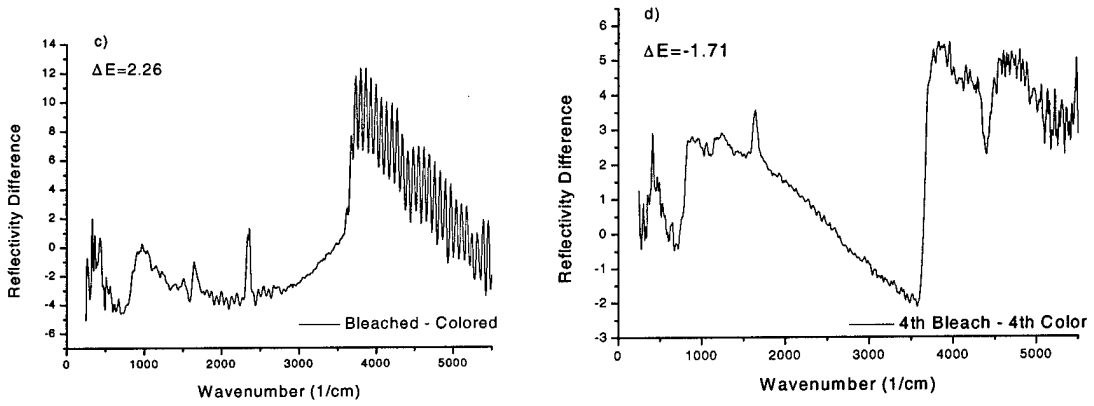

Figure 4: The difference in reflectance between the two operating states of Device #1 (H^+ions) a) First Cycle b) Second Cycle c) Third Cycle d) Fourth Cycle.

II) Device #2 (H^+ions)

For this device 95% of the blackbody region was covered in the measurement.

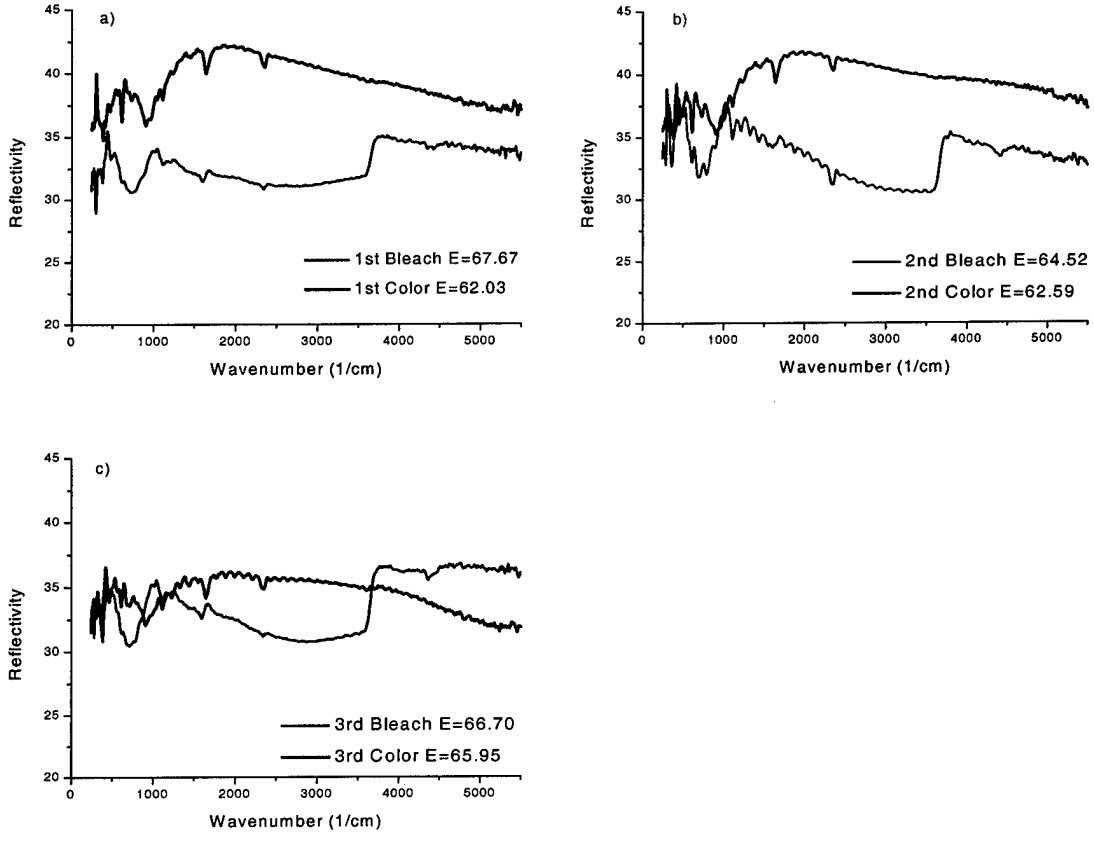

Figure 5: The measured reflectance of Device #2 (H^+ions) ——with the top c-WO_3 unintercalated (bleached) and ▬ with the top c-WO_3 intercalated (colored). a) First Cycle b) Second Cycle c) Third Cycle

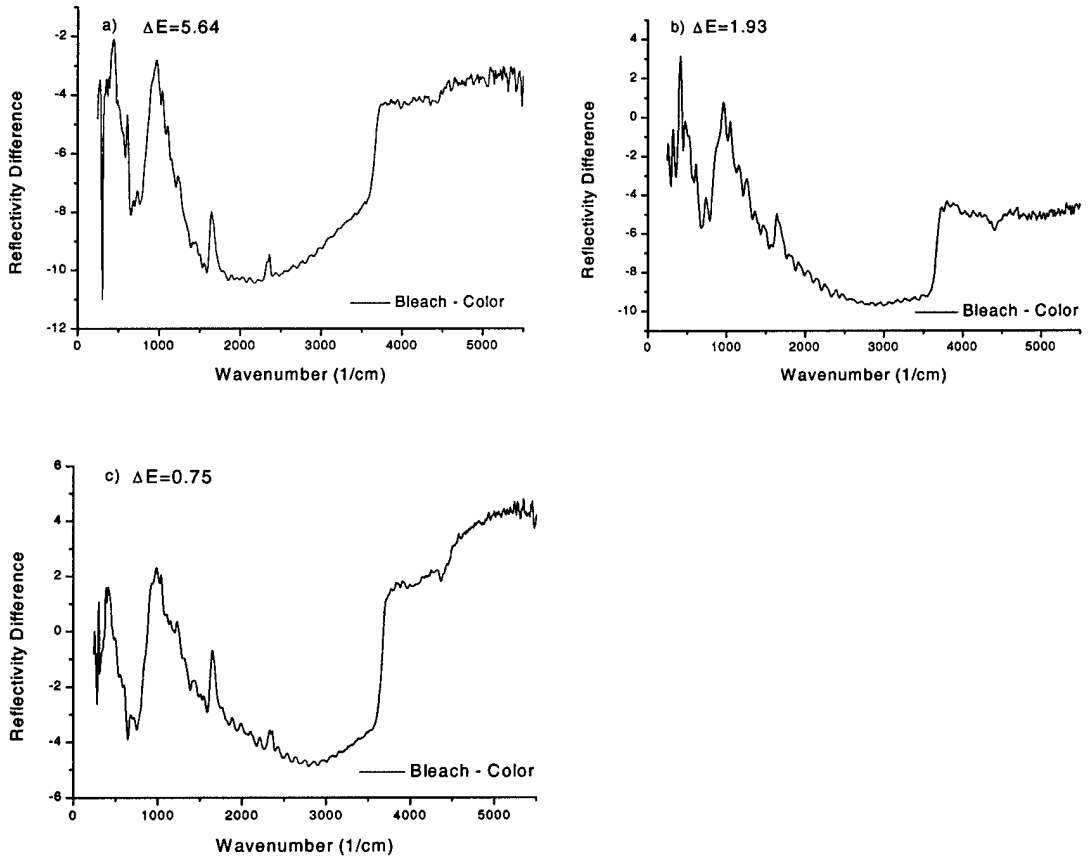

Figure 6: The difference in reflectance between the two operating states of Device #2 (H^+ions) a) First Cycle b) Second Cycle c) Third Cycle

III) Device #3 (H^+ions)

For this device 95% of the blackbody region was covered in the measurement.

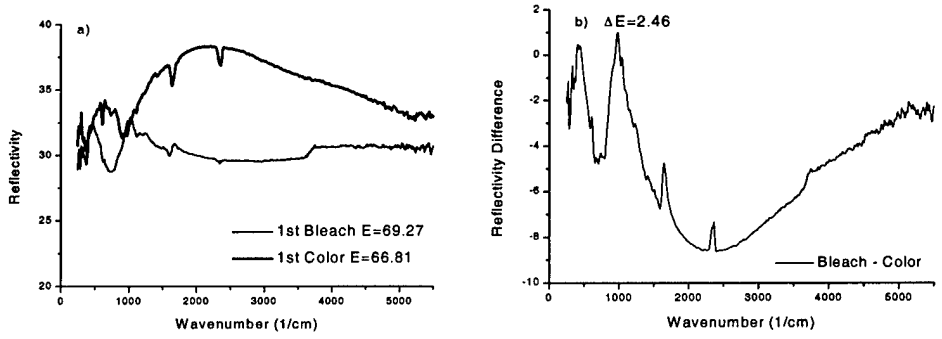

Figure 7: a) The measured reflectance of Device #3 (H^+ions) ——with the top c-WO_3 unintercalated (bleached) and —— with the top c-WO_3 intercalated (colored). b) The difference in reflectance between the two operating states of the device.

DEVICES UTILIZING Li^+ IONS

The following devices had the same structure as Devices #1-3, however for Devices #4-7 the intercalant ion was changed to Li^+

IV) Device #4 (Li^+ Ions)

For this device 95% of the blackbody region was covered in the measurement.

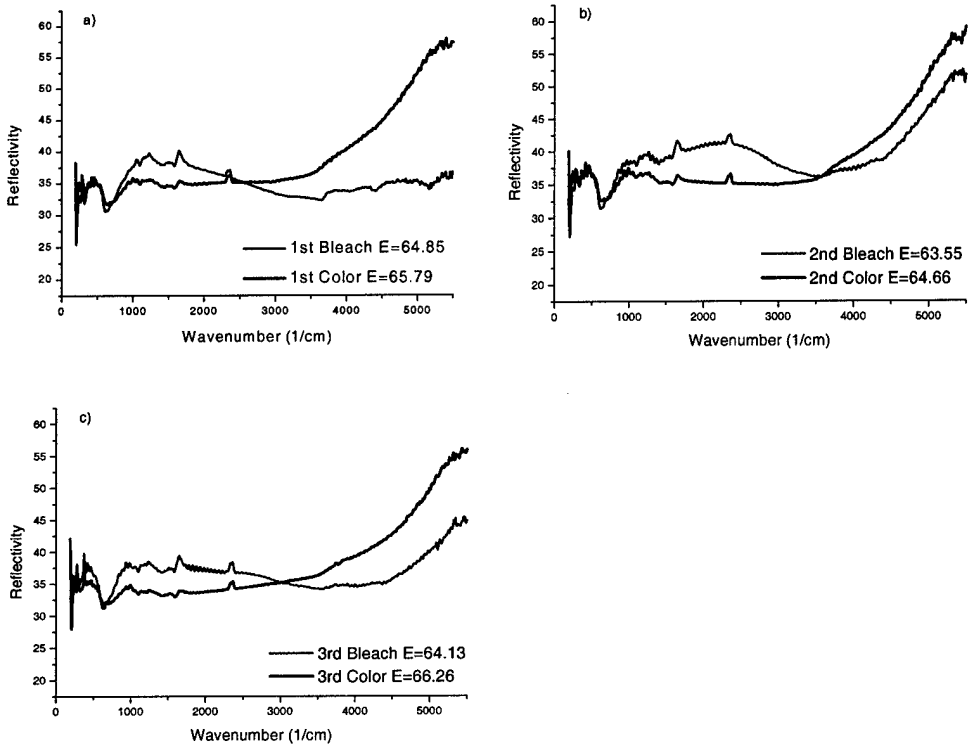

Figure 8: The measured reflectance of Device #4 (Li^+ Ions) ━━ with the top c-WO_3 unintercalated (bleached) and ━━ with the top c-WO_3 intercalated (colored). a) First Cycle b) Second Cycle c) Third Cycle

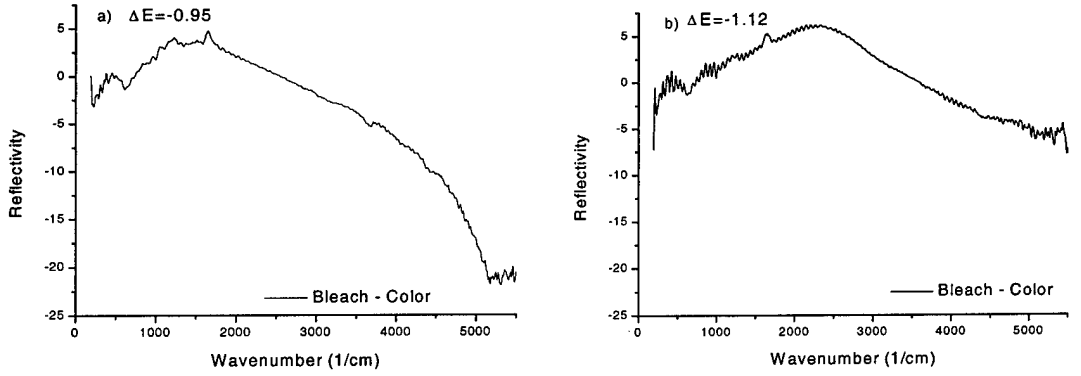

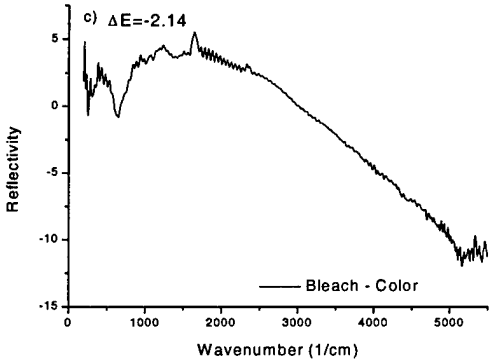

Figure 9: The difference in reflectance between the two operating states of Device #4 (Li^+ Ions). A) First Cycle b) Second Cycle c) Third Cycle

V) Device #5 (Li^+ Ions)

For this device 95% of the blackbody region was covered in the measurement.

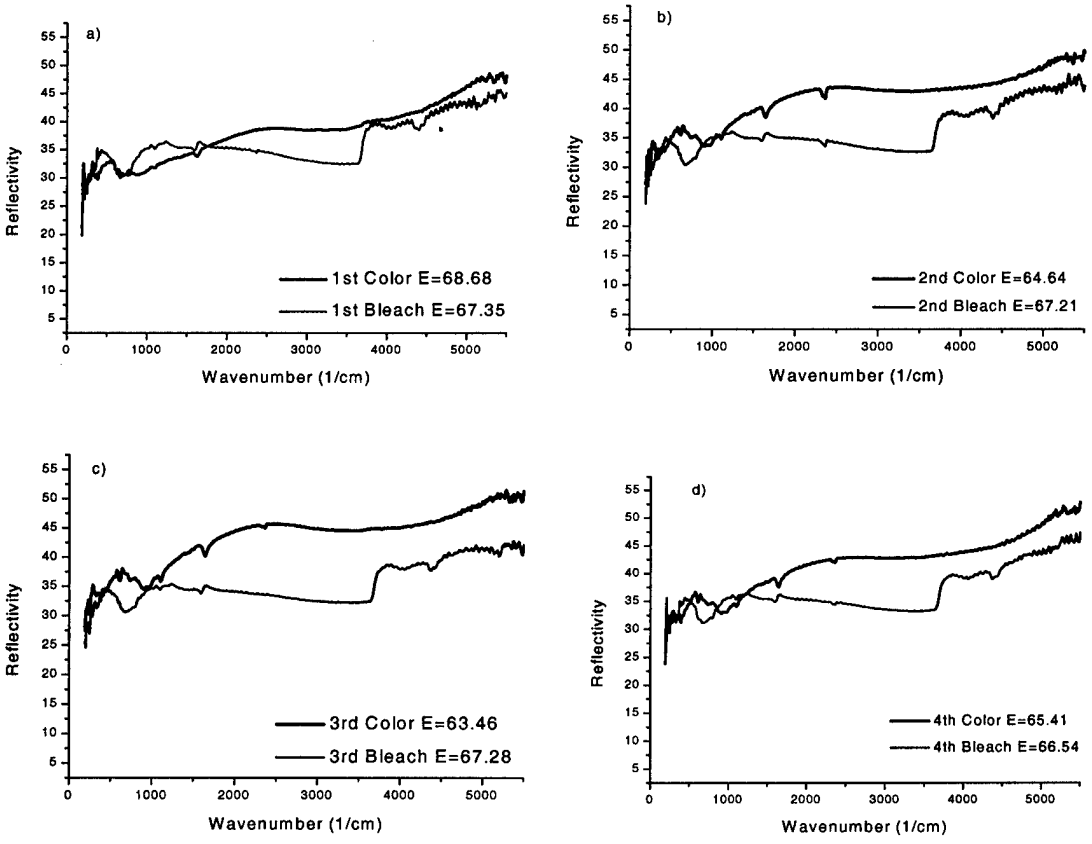

Figure 10: The measured reflectance of Device #5 (Li^+ Ions)—— with the top c-WO_3 unintercalated (bleached) and —— with the top c-WO_3 intercalated (colored). a) First Cycle b) Second Cycle c) Third Cycle d)Fourth Cycle

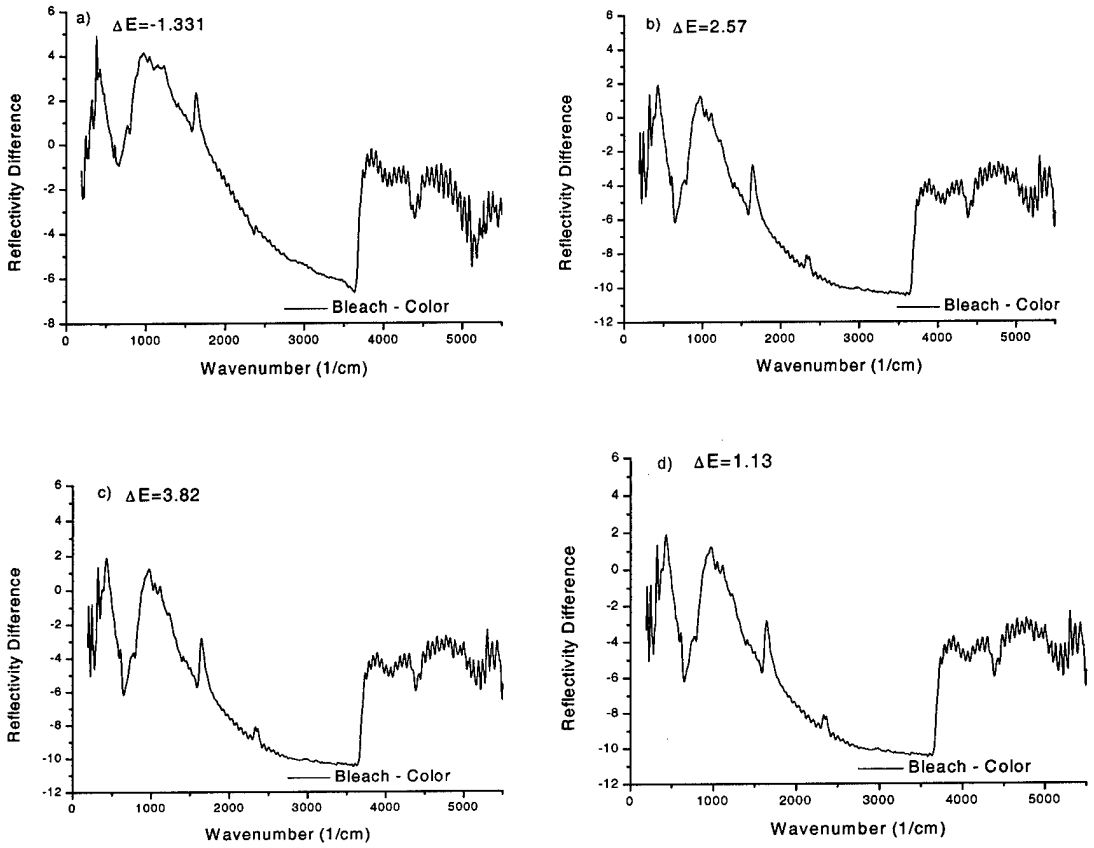

Figure 11: The difference in reflectance between the two operating states of Device #5 (Li^+ Ions) . a) First Cycle b) Second Cycle c) Third Cycle d) Fourth Cycle

VI) Device #6 (Li^+ Ions)

For this device 95% of the blackbody region was covered in the measurement.

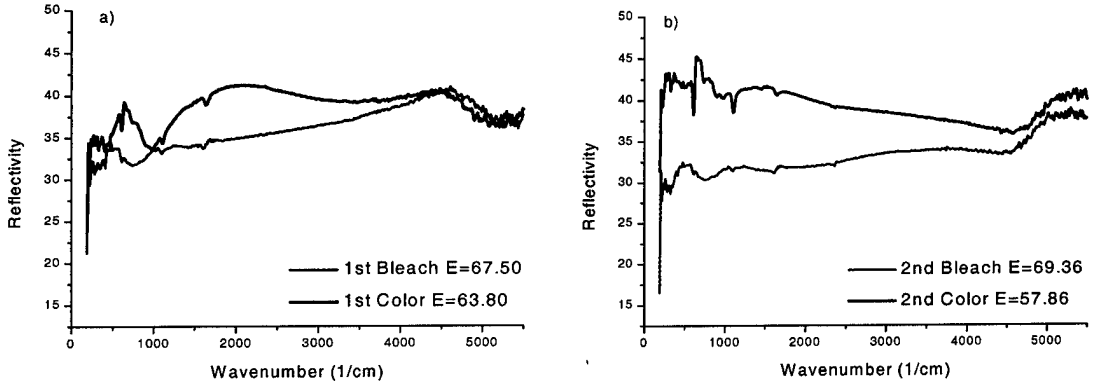

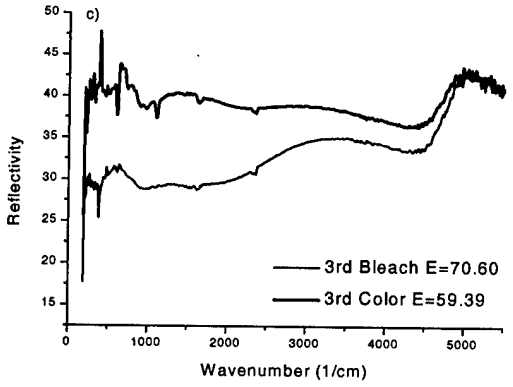

Figure 12: The measured reflectance of Device #6 (Li^+ Ions) —— with the top c-WO_3 unintercalated (bleached) and —— with the top c-WO_3 intercalated (colored). a) First Cycle b) Second Cycle c) Third Cycle

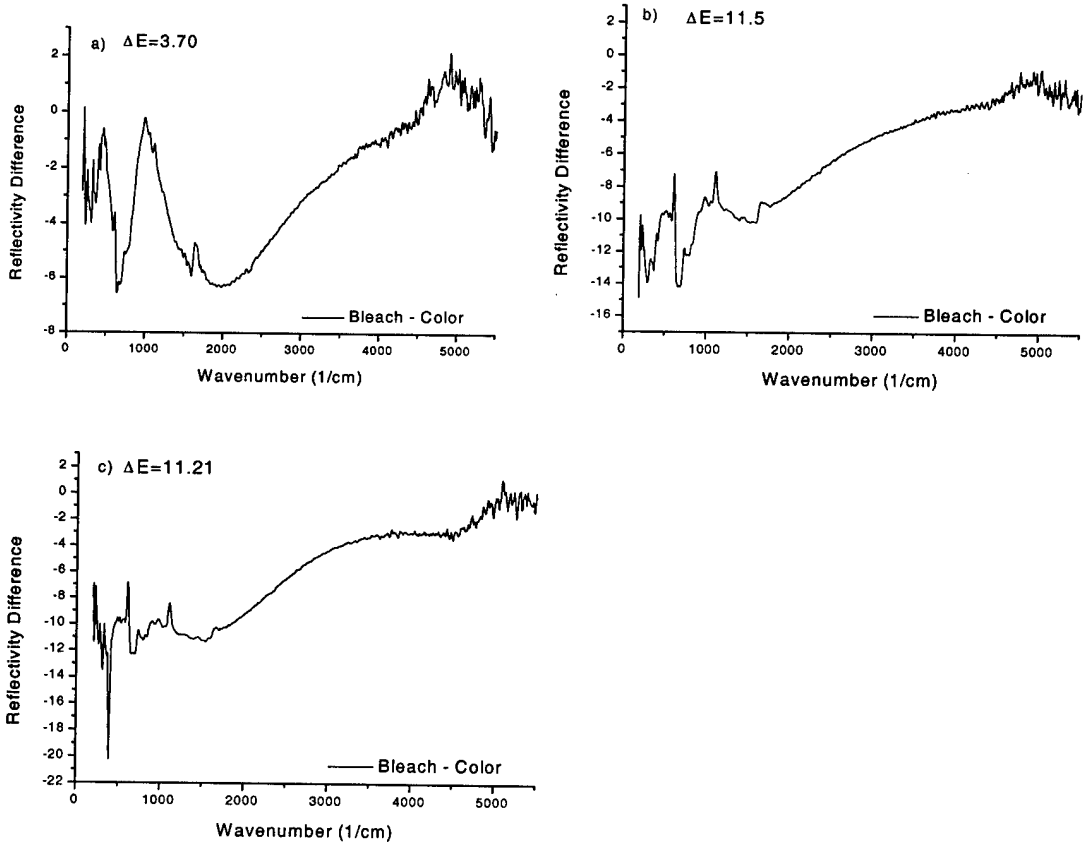

Figure 13: The difference in reflectance between the two operating states of Device #6 (Li^+ Ions). a) First Cycle b) Second Cycle c) Third Cycle

VII) Device #7 with (Li^+ Ions)

For this device 92% of the blackbody region was covered in the measurement.

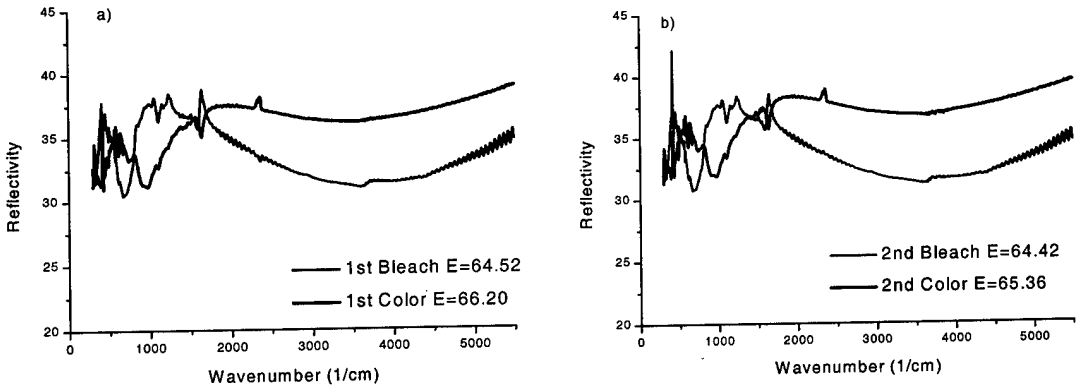

Figure 14: The measured reflectance of Device #7 (Li^+ Ions) with ▬ the top c-WO_3 unintercalated (bleached) and with ▬ the top c-WO_3 intercalated (colored). a)First Cycle b) Second Cycle

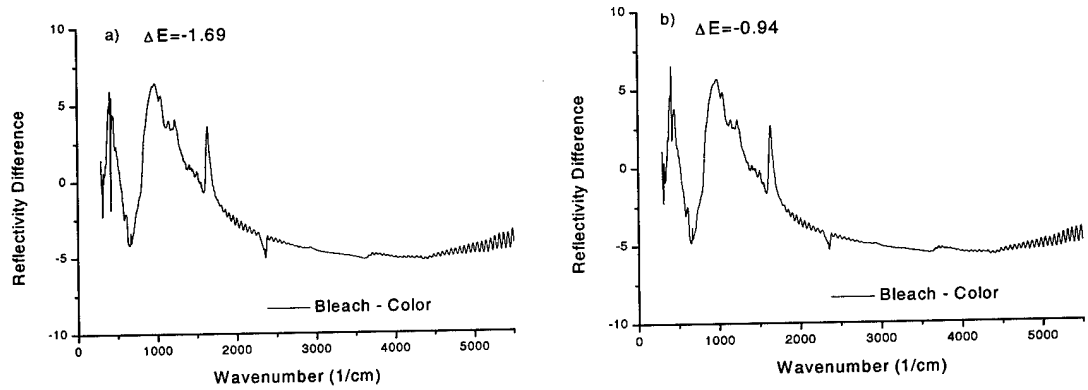

Figure 15: The difference in reflectance between the two operating states of Device #7 (Li^+ Ions). a) First Cycle b) Second Cycle

D) PERFORMANCE OF POLYMER-BASED DEVICES WITH DLC ANTIREFLECTION COATINGS

INTRODUCTION

There have also been two modifications to the Basic polymer device structure. The first of which is an addition of a diamond like carbon (DLC) film as an IR anti-reflection coating on top of the silicon. The structure of this device is shown in Figure 16.

DLC reduces reflectance from Si over a range of wavelengths centered at 10μm. This helps improve c-WO_3 switching near 10μm (1000cm^{-1}), that is, near the room

temperature blackbody peak. This "anti-reflection" coating central wavelength can be mouved by changing DLC thicknesses.

DLC coating index of refraction = n_1
Si Surface index of refraction = n_0

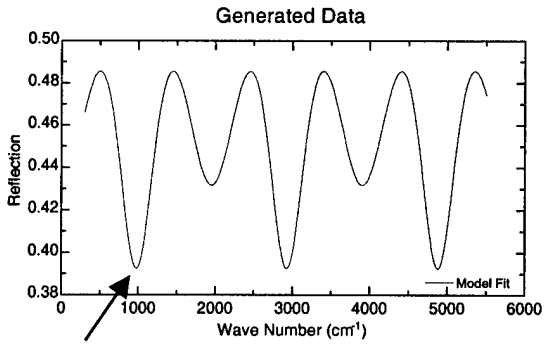

10μm

If $n_0 = \sqrt{n_1}$ then it is possible to chose a thickness for the DLC coating such that thickness = $\lambda_{min}/4n_1$
where λ_{min} is the wavelength at which reflection is a minimum. In this case $\lambda_{min} = 10\mu m$

The DLC coating works because the index of refraction of Si is approximately equal to the square root of the index of DLC at 10μm. By choosing the thickness according to the equation above we can tune the wavelength at which the lowest reflectance, or highest emittance occurs. The above simulation shows the results of the reflection spectra if $n_1 = 1.88$ $n_0 = 3.5$ (the approximate index of refraction for DLC, obtained from analysis of a commercial film, and Si at 10μm respectively) and t=1.6μm. With these conditions the reflectivity of the surface is minimized at the 10μm region.

STRUCTURE

Figure 16 shows the structure of Device #8 DLC coated polymer-based device (Li^+ions)

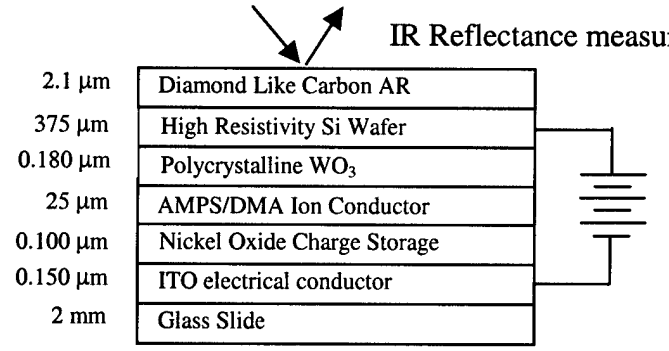

Figure 16: Structure of polymeric ion conducting device, with DLC AR coating including the location of the electrical contacts to the external source and the method in which the reflectance measurement was taken

PERFORMANCE

Device #8 DLC coated polymer-based device (Li^+ ions)

For this device 95% of the blackbody region was covered in the measurement.

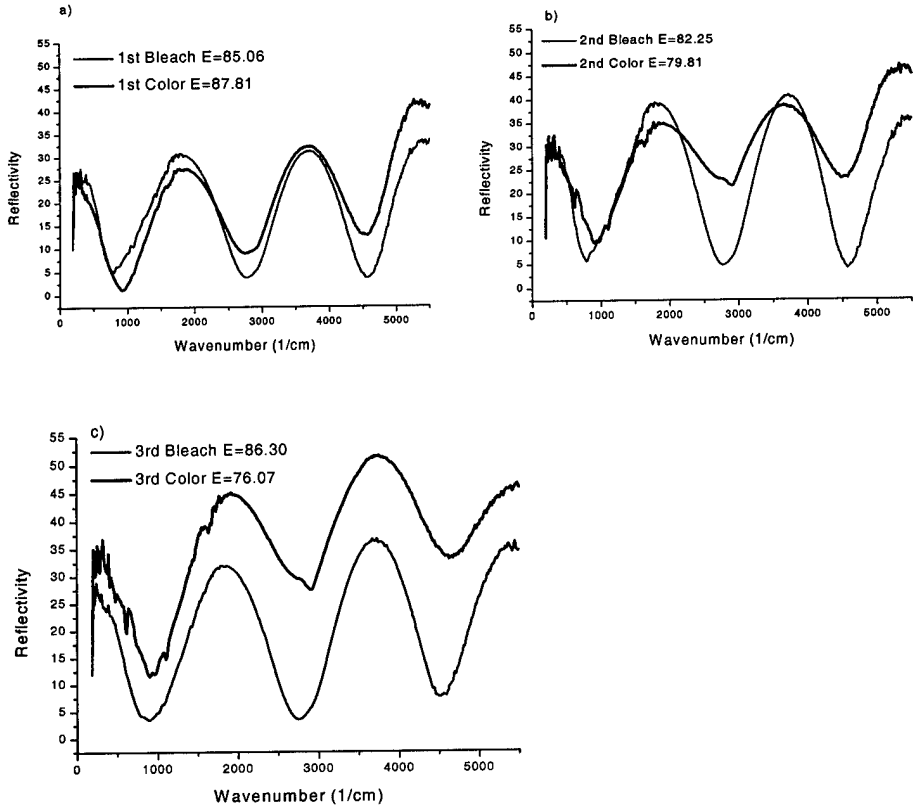

Figure 17: The measured reflectance of Device #8 DLC coated polymer-based device (Li^+ ions) with ▬ the top c-WO_3 unintercalated (bleached) and with ▬ the top c-WO_3 intercalated (colored). a)First Cycle b) Second Cycle c) Third Cycle

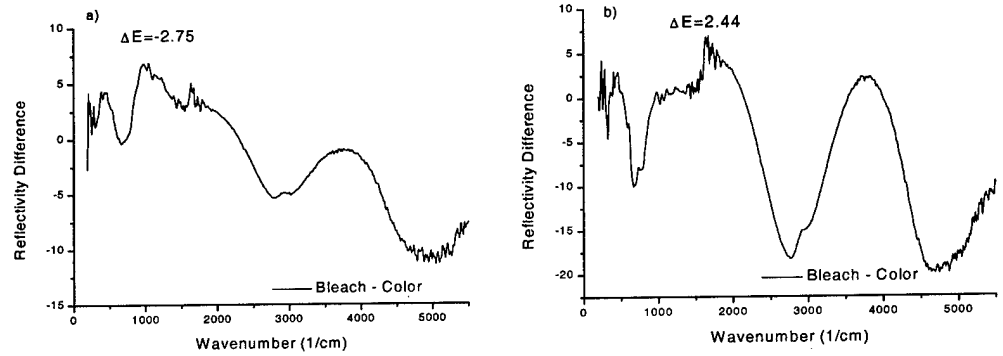

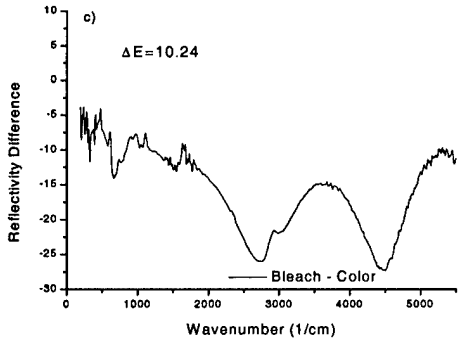

Figure 18: The difference in reflectance between the two operating states of Device #8 DLC coated polymer-based device (Li^+ ions). a) First Cycle b) Second Cycle c) Third Cycle

The DLC AR coating had a large effect on measured device performance. This is especially true for the third cycle which had a $\Delta E = 10.24$. The reason for this improvement is the DLC imparted a broad minimum in the measured reflectance of the device near 10μm. The portion of the light reflected from the sample is inversely proportional to the light that is emitted. Due to the increase in light reaching the c-WO_3 the device was more effective in its emittance modulation.

E) PERFORMANCE OF POLYMER DEVICES WITH VANADIUM OXIDE STORAGE LAYER

INTRODUCTION

The second modification was a change to the material used for the charge storage layer. Instead of using nickel oxide a vanadium oxide material was utilized. Vanadium oxide is often used in solid state battery research where Li^+ is the mobile ion species.

STRUCTURE

Figure 19 shows the structure of this device.

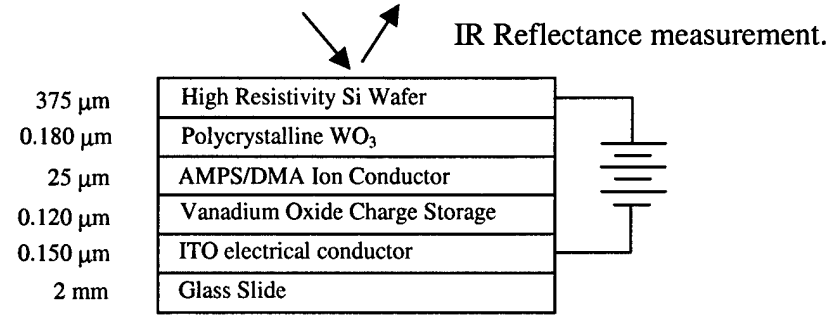

Figure 19: Structure of polymeric ion conducting device, with Vanadium Oxide storage layer including the location of the electrical contacts to the external source and the method in which the reflectance measurement was taken

PERFORMANCE

Device #9 polymer –based device with Vanadium Oxide (Li^+ ions)

For this device 75% of the blackbody region was covered in the measurement.

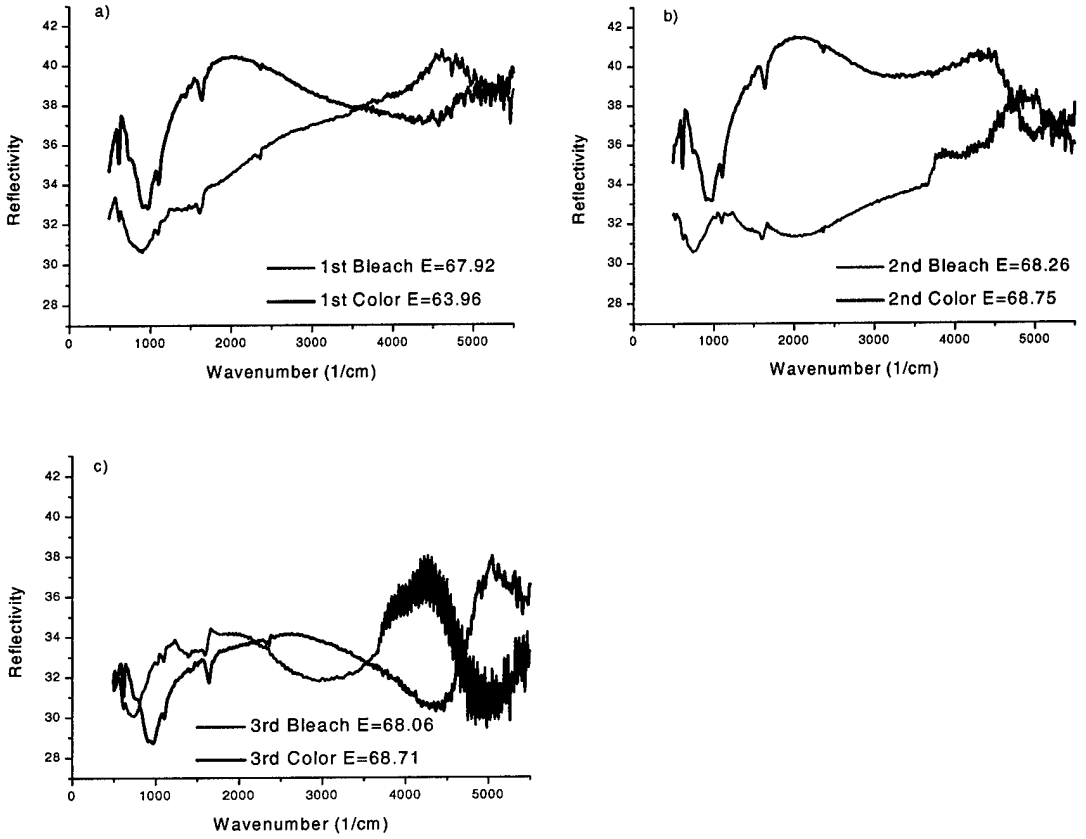

Figure 20: The measured reflectance Device #9 polymer –based device with Vanadium Oxide (Li^+ ions) with ▬ the top c-WO_3 unintercalated (bleached) and with ▬ the top c-WO_3 intercalated (colored). a)First Cycle b) Second Cycle c) Third Cycle

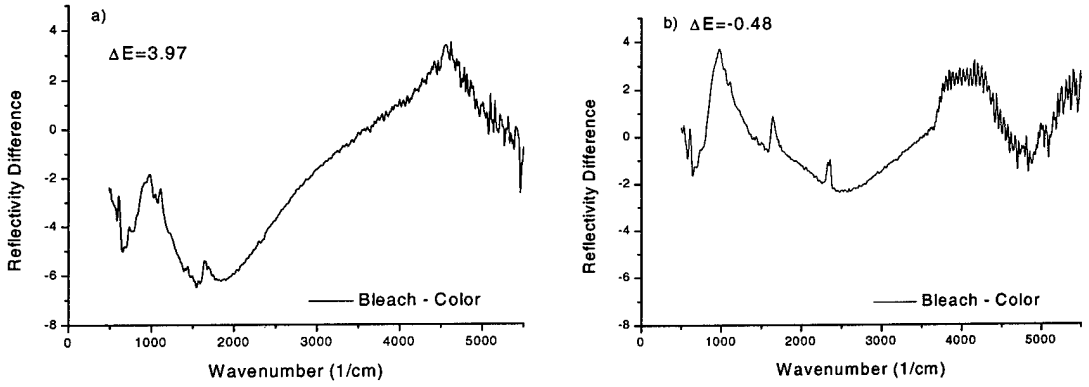

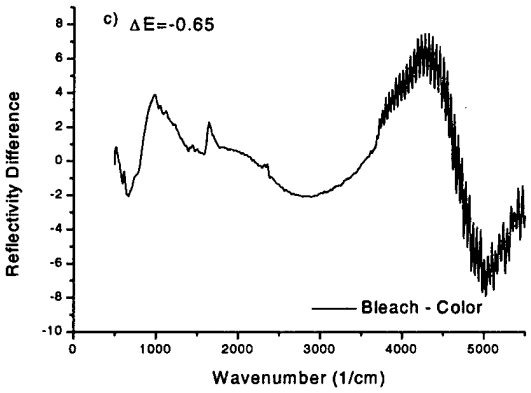

Figure 21: The difference in reflectance between the two operating states Device #9 polymer – based device with Vanadium Oxide (Li^+ ions). a) First Cycle b)Second Cycle c) Third Cycle.

Table 1 Summary of Polymer-based Device Performance.

Device Index	% of blackbody covered	Cycle #	Emittance with c-WO_3 Bleached	Emittance with c-WO_3 Colored	Change in Emmissivity	% Change in Emmissivity (relative to bleached)
Device #1 (H^+ions)	95	1	62.65	61.45	1.21	1.93%
		2	60.84	59.14	1.70	2.79%
		3	60.66	58.40	2.26	3.73%
		4	61.54	63.26	-1.71	-2.78%
Device #2 (H^+ions)	95	1	67.67	62.03	5.64	8.33%
		2	64.52	62.59	1.93	2.99%
		3	66.70	65.95	0.75	1.12%
Device #3 (H^+ions)	95	1	69.27	66.81	2.46	3.55%
Device #4 (Li^+ions)	95	1	64.85	65.79	-0.94	-1.45%
		2	63.55	64.66	-1.11	-1.75%
		3	64.13	66.26	-2.14	-3.34%
Device #5 (Li^+ions)	95	1	67.35	68.68	-1.33	-1.97%
		2	67.21	64.64	2.57	3.82%
		3	67.28	63.46	3.82	5.68%
		4	66.54	65.41	1.13	1.70%
Device #6 (Li^+ions)	95	1	67.50	63.80	3.69	5.47%
		2	69.36	57.86	11.50	16.58%
		3	70.60	59.39	11.21	15.88%
Device #7 (Li^+ions)	92	1	64.52	66.20	-1.69	-2.62%
		2	64.42	65.36	-0.94	-1.46%
Device #8 DLC Coated polymer-based (Li^+ions)	95	1	85.06	87.81	-2.75	-3.23%
		2	82.25	79.81	2.44	2.97%
		3	86.30	76.07	10.24	11.87%
Device #9 Polymer-based device with Vanadium Oxide Storage Layer (Li^+ions)	75	1	67.92	63.96	3.97	5.85%
		2	68.26	68.75	-0.48	-0.70%
		3	68.06	68.71	-0.65	-0.96%

PART IV: MONOLITHIC ALL VACUUM FABRICATED DEVICES

A) INTRODUCTION

The other category of devices fabricated during this contract were monolithic multilayer stacks. These were sputter deposited on to single substrates (recall that two substrates were needed for polymer-based devices). All-vacuum fabricated device manufacturing is relatively easily scaled up to make large area devices. It has been a major goal of the contract to develop these type of devices.

For space applications these devices also have the added benefit of being more durable to the low earth orbit (LEO) environment. In LEO polymer degradation caused by UV light and atomic oxygen is a significant problem. Even with monolithic devices UV light is a potential device performance inhibitor because many electrochromic materials, including WO_3 and Vanadium Oxide are photochromic materials. Photochromic materials are materials that have varying optical characteristics caused by exposure to UV radiation.

When a large area electrochromic device is developed for space applications it will be necessary to study its durability under LEO conditions.

B) FABRICATION

These devices were deposited on several different substrates. If the substrate was a high resistance (low dopant concentration) silicon wafer, then the c-WO_3 was deposited first. Over this a Tantalum Oxide film was deposited. Often the c-WO_3 would be electrochemically intercalated. Then a Nickel Oxide charge storage layer was deposited, and finally an ITO layer was deposited as a transparent conducting layer. If the substrate was a glass slide, the order of deposition was reversed so that c-WO_3 was always on top. All the monolithic devices utilized Li^+ as a mobile ion. The use of Li^+ allowed more time to process the device and deposit the other device layers after the device had been intercalated electrochemically

C) PERFORMANCE OF BASIC MONOLITHIC DEVICES

VISIBLE DEVICE: STRUCTURE AND TESTING

Before attempting to make an IR modulating device, a visible operating device, designed to modulate transmitted light, was made with the structure shown in Figure 22. Figure 23 shows the visible transmittance change in such a device. The success of this encouraged us to continue our work with the monolithic structures because the materials are all the same and the only modification would be made with the substrate. Electrical contact was made to the ITO|Glass with an alligator clip and banana plug. The other electrical contact was made to the top ITO layer by first applying an electrically insulating paint to a small area of the device, and then over this a silver paint was applied

in such a way that an alligator clip attached to the silver paint was in contact with the top ITO. Figure 22 shows the structure of the device.

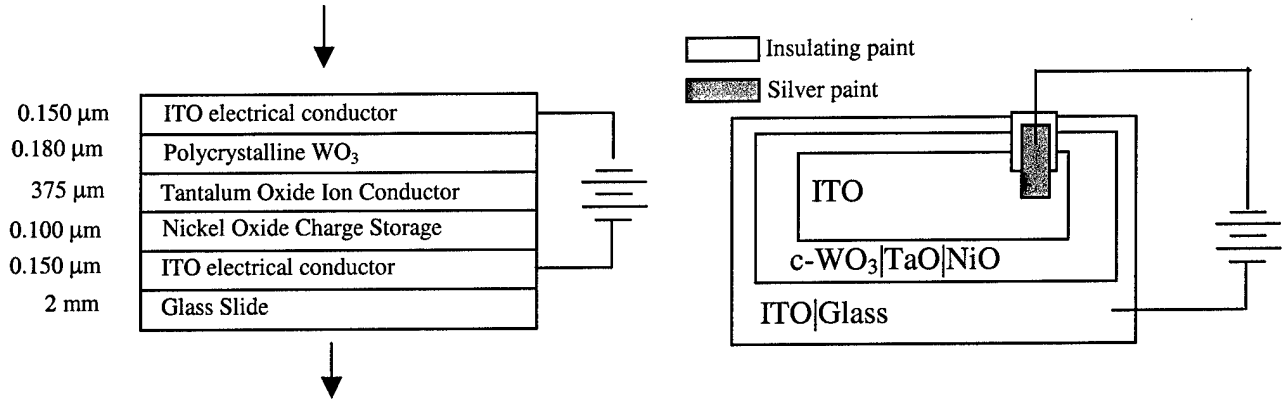

Figure 22 Monolithic device structure, including the location of the electrical contacts to the external source.

VISIBLE DEVICE: PERFORMANCE

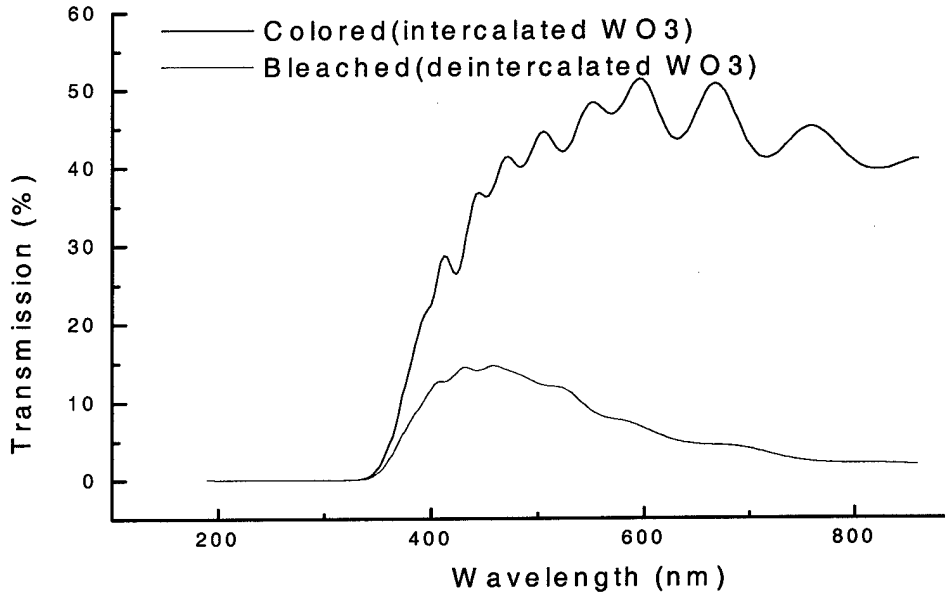

Figure 23: Transmittance modulation of Visible operating monolithic device

INFRARED DEVICE: STRUCTURE

Figure 24 shows the structure of one of the Basic Monolithic devices we have made for IR modulation:

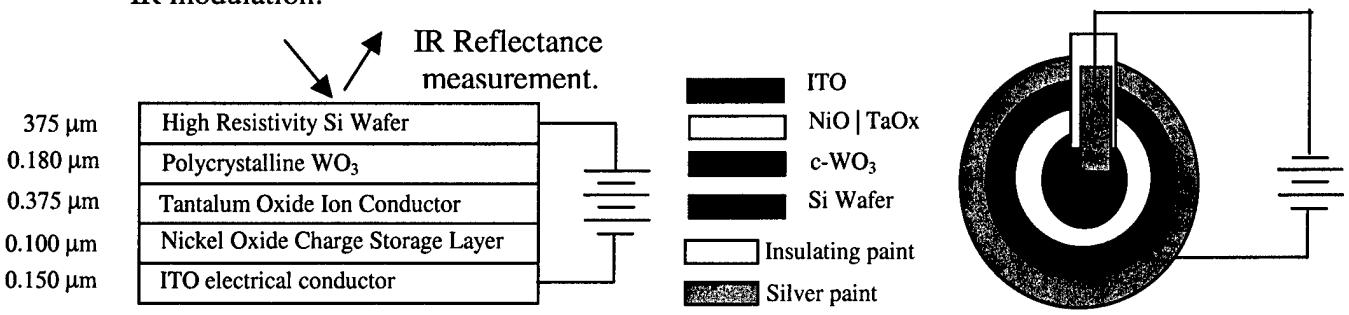

Figure 24: Monolithic device structure, including the location of the electrical contacts to the external source and the method in which the reflectance measurement was taken.

INFRARED DEVICE: PERFORMANCE

I) Device #1

For this device 75% of the blackbody region was covered in the measurement.

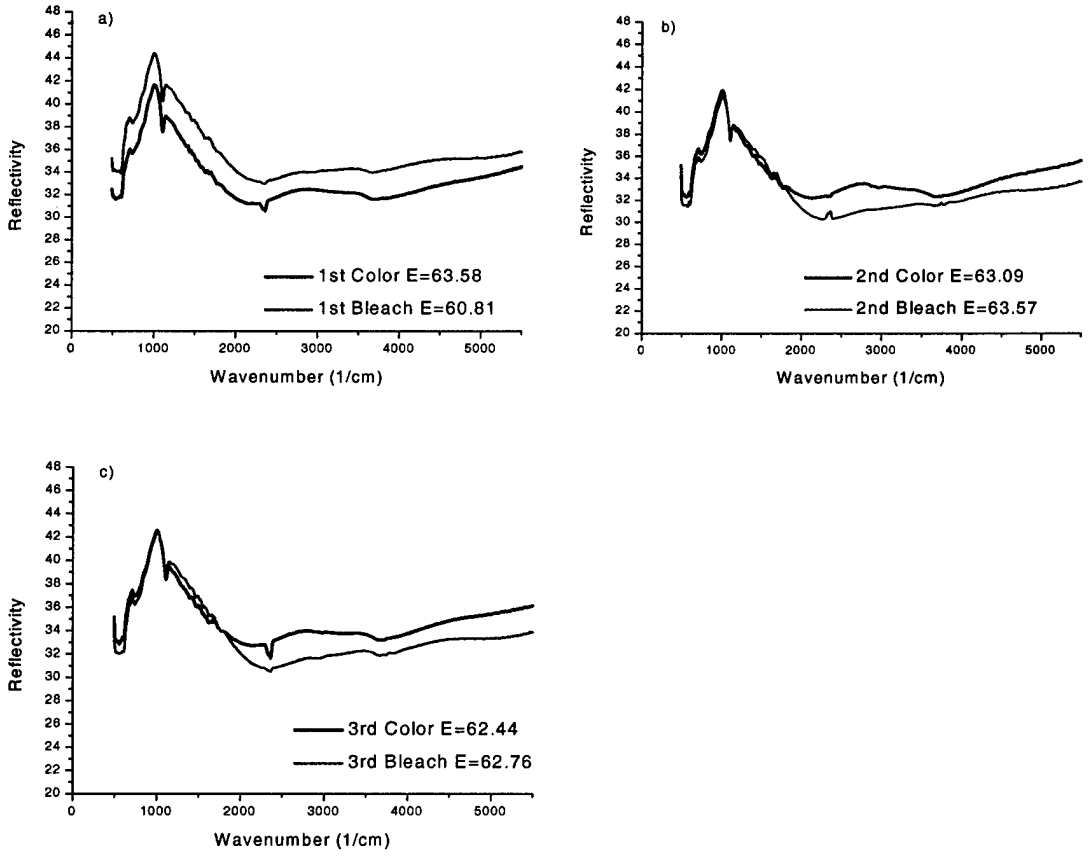

Figure 25: The measured reflectance of Device #1 ——with the c-WO_3 unintercalated (bleached) and —— with the top c-WO_3 intercalated (colored). a) First Cycle b) Second Cycle c) Third Cycle

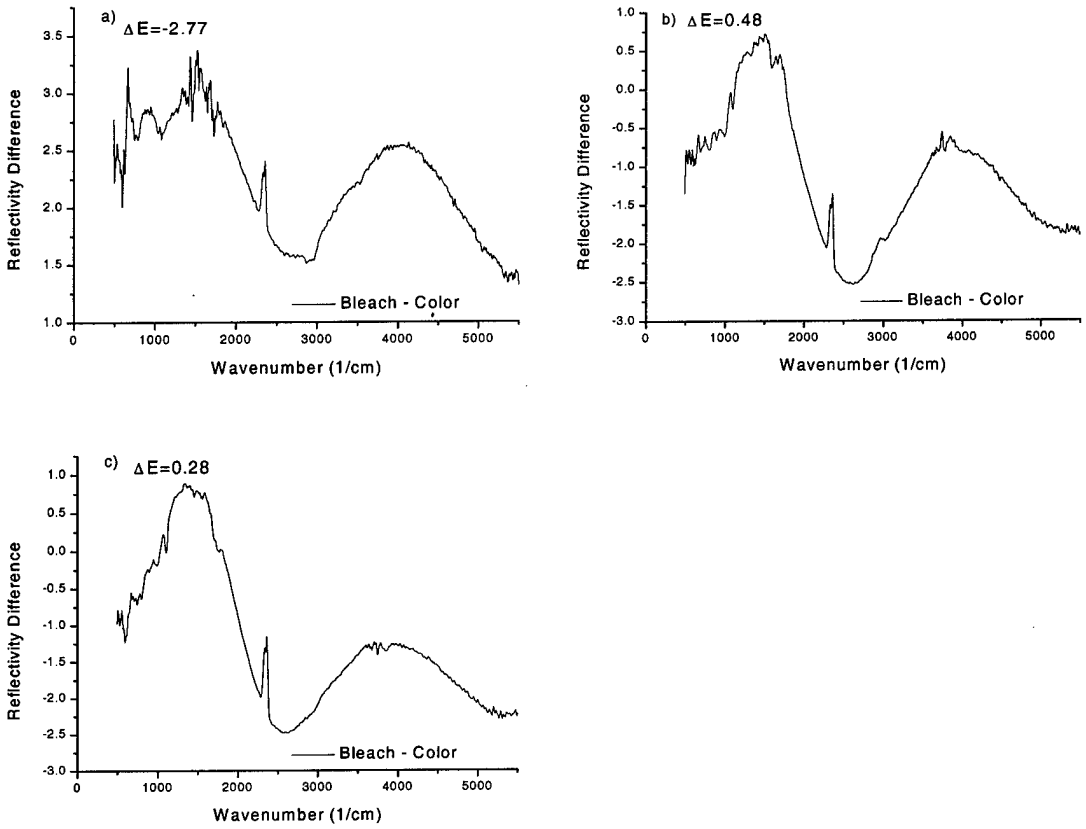

Figure 25: The difference in reflectance between the two operating states of Device #1. a) First Cycle b) Second Cycle c) Third Cycle

II) Device #2

For this device 92% of the blackbody region was covered in the measurement.

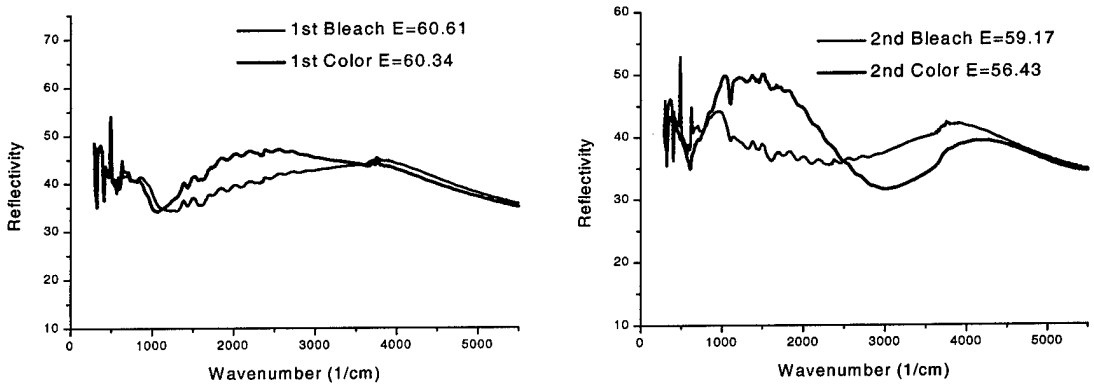

Figure 26: The measured reflectance of Device #2 ▬with the c-WO_3 unintercalated (bleached) and▬ with the top c-WO_3 intercalated (colored). a) First Cycle b) Second Cycle

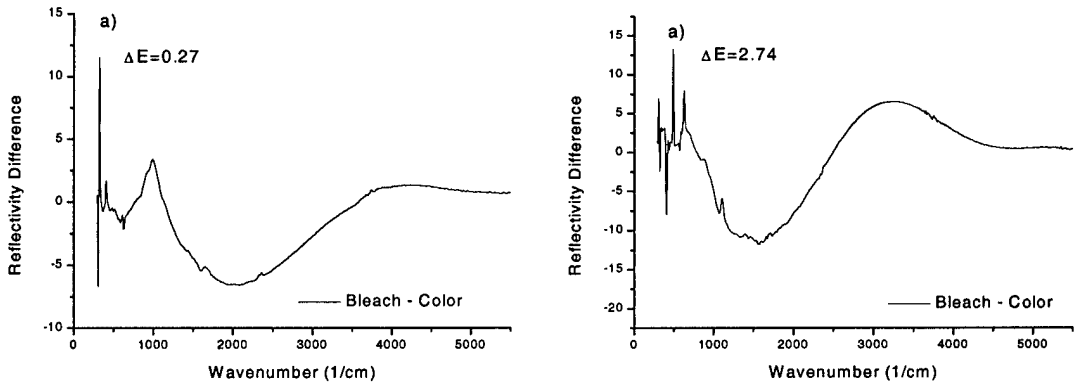

Figure 27: The difference in reflectance between the two operating states of Monolithic Device #2. a) First Cycle b) Second Cycle

D) PERFORMANCE OF MONOLITHIC DEVICES WITH THIN CONDUCTING TOP LAYER

INTRODUCTION

The difficulty with the devices measured through the silicon substrate is that a significant portion of the IR probe beam is reflected off of the Si|Air interface before the beam makes it to the device we are trying to measure. In order to get a better idea of the modulation taking place due to the device the probe beam needs to be directly reflected off of the top c-WO_3 layer. The first attempt at accomplishing this was to utilize a very thin electrical conducting layer in hope that a majority of the beam would penetrate through the thin IR reflective conductor.

To simplify the fabrication process an amorphous WO_3 layer was used as an ion storage layer. This eliminated one of the chamber pump-downs decreasing the fabrication time from 5 days to three days.

STRUCTURE

Figure 28 shows the structure of this device deposited on a glass slide coated with ITO.

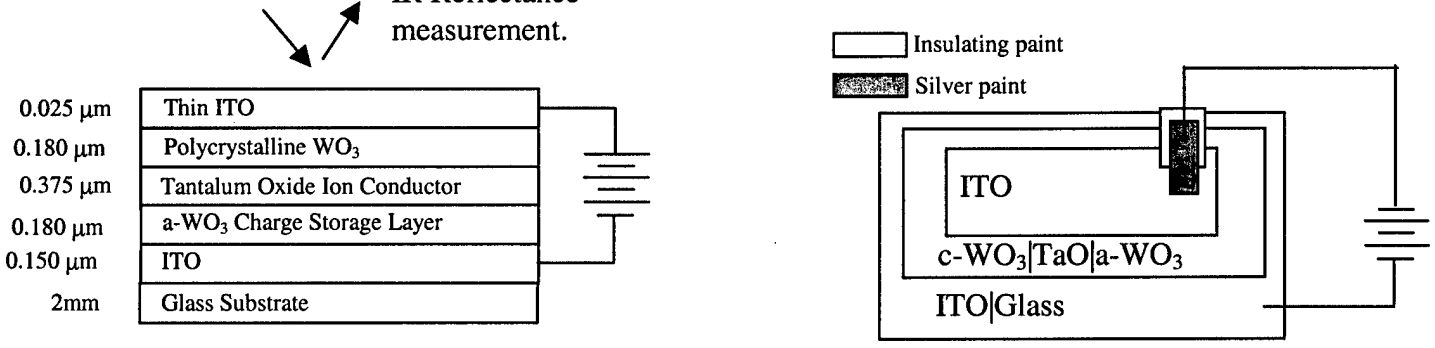

Figure 28: Structure of monolithic device with a thin conducting layer covering the c-WO_3

PERFORMANCE

I) Device #3 (Thin Conducting Top Layer)

The following figures show the results of measurements taken on this device. This device showed good promise. However, after the first cycle it no longer showed any change in reflectivity. For this device 92% of the blackbody region was covered in the measurement.

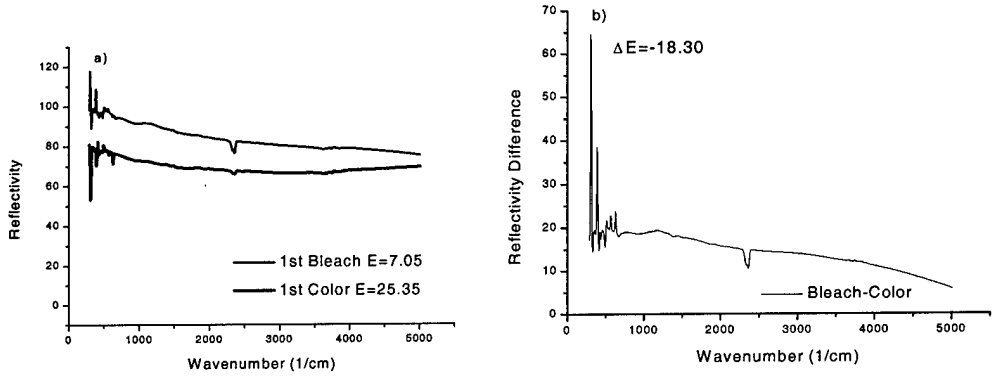

Figure 29 a) The measured reflectance of Device #3 (Thin Conducting Top Layer) with ▬ the top c-WO_3 unintercalated (bleached) and ▬ with the top c-WO_3 intercalated (colored). b) The difference in reflectance between the two operating states of the device.

FAILURE ANALYSIS

Another device similar to this one was deposited on a Si substrate instead of an ITO coated glass slide. The device failed to show any reflectivity change at all. This sample was sent to Leipzig, Germany where Secondary Neutron Mass Spectroscopy (SNMS) was used to give a depth profile. This technique involves sputtering the sample and then using a mass spectrometer to determine what is coming from the sample. This was done in an attempt to determine why the device failed to cycle. Figure 30 shows the data obtained from this experiment. One possible reason for the device failure is the Li^+ ion is getting trapped at the thin film interfaces. The intensity of the Li signal increases at the interface between c-WO_3 and Tantalum Oxide, then again at the interface between the Si substrate and the a-WO_3 film. The interfaces with the highest concentration are indicated by the green vertical lines.

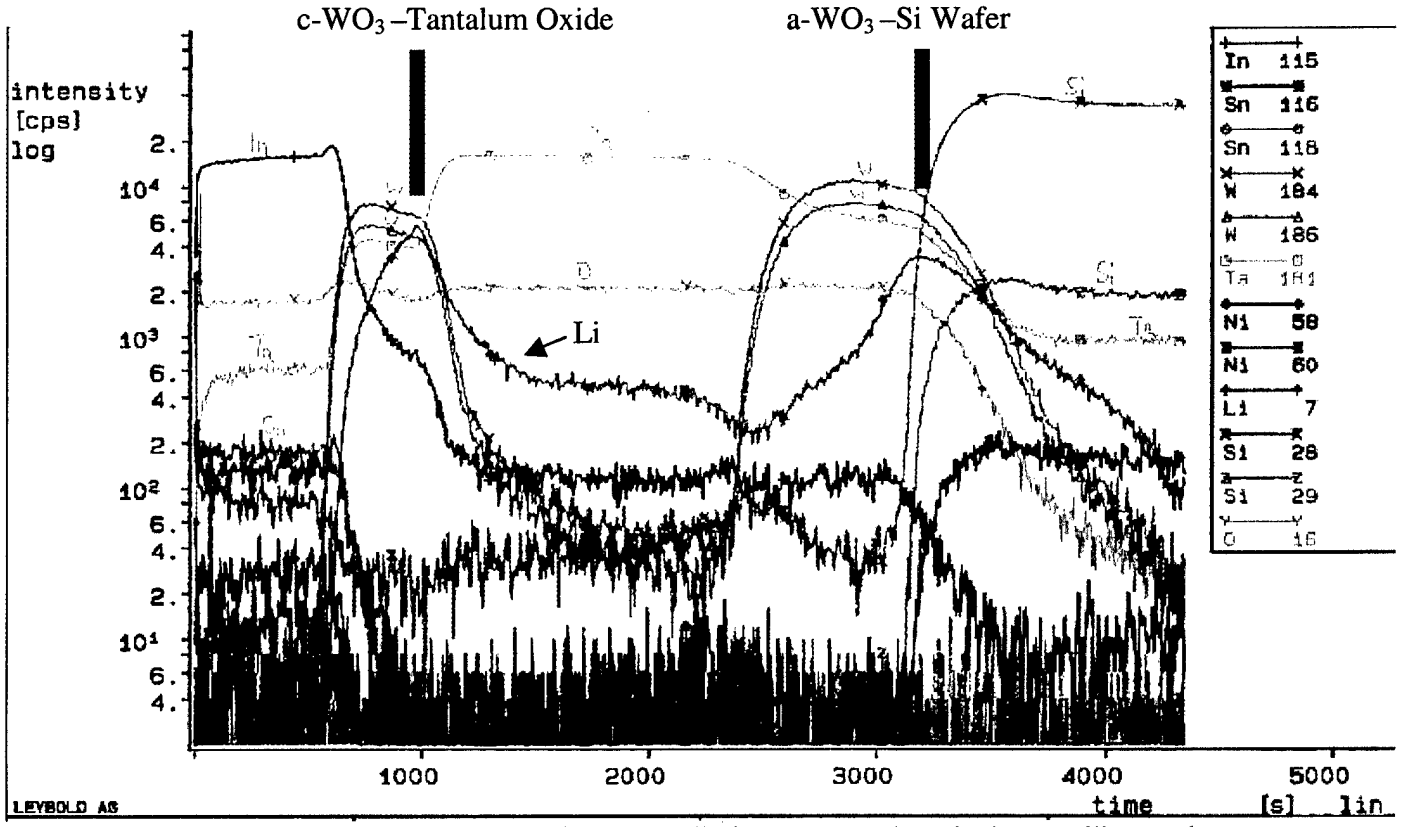

Figure 30: SNMS depth profiling for a monolithic structure, deposited on a silicon substrate, with a thin ITO film on top

E) PERFORMANCE OF MONOLITHIC DEVICES WITH CONDUCTING GRID

INTRODUCTION

Other investigations involved the use of grids as electrical conductors. A successful electrochromic stack utilizes two electrically conducting films as the top and bottom layers of the device. However electrical conductors are generally IR reflective. Covering the c-WO_3 with an electrically conducting film negates any IR optical modulation contributed by the rest of the device. An attempt to overcome this obstacle was made using a metallic grid on top of the c-WO_3. If the grid covers less than 10% of the top area of the device than the majority of the IR probe could penetrate through to the rest of the device.

FABRICATION AND STRUCTURE

Photolithography with a negative photoresist was used to make the grids. The line widths were 10μm, wide with a distance of 500μm between each line. The metal used for the grids was Aluminum and the metal layer at the base of the device was either Al or Cr.

Figure 31 shows the structure of this device on a glass slide.

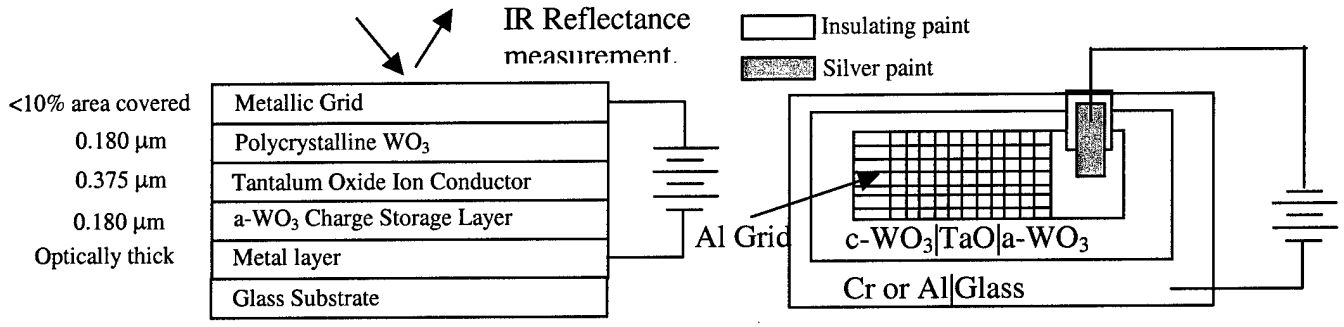

Figure 31: Structure of monolithic device with a metallic grid covering the c-WO_3.

I) Device #4 (Aluminum Conducting Grid)

For this device 95% of the blackbody region was covered in the measurement.

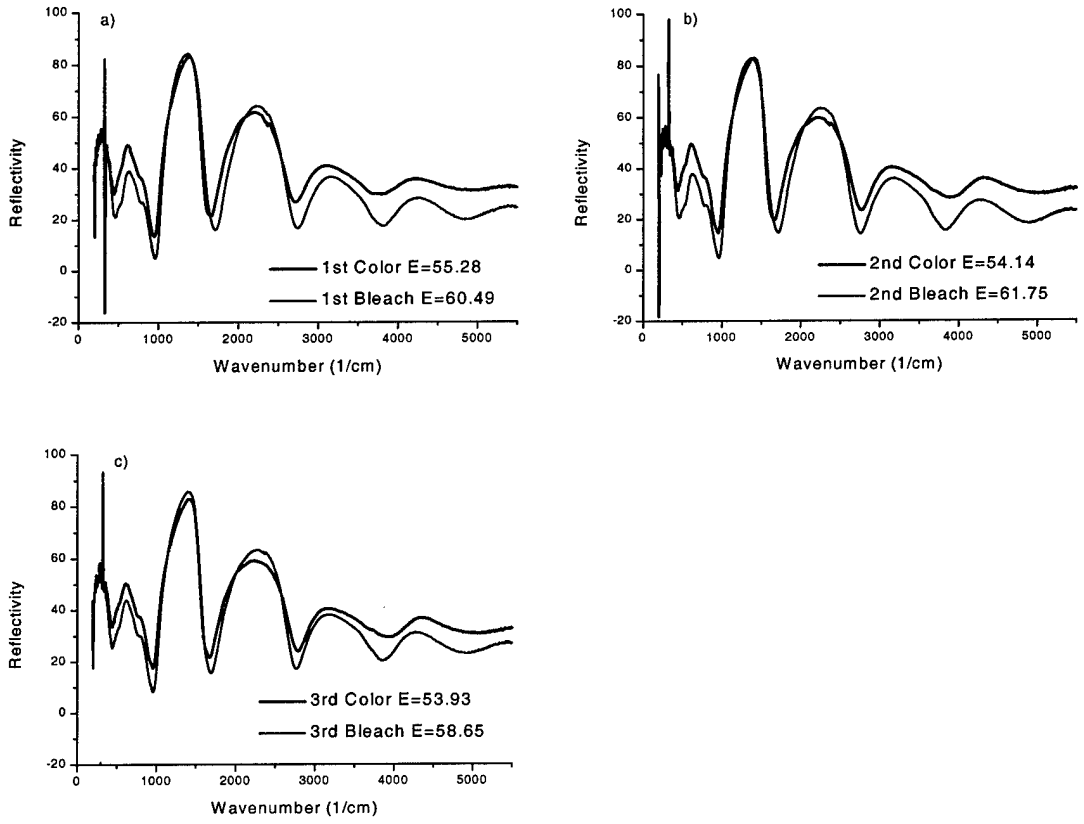

Figure 32: The measured reflectance of Device #4 (Aluminum Conducting Grid) ——— with the c-WO_3 unintercalated (bleached) and ——— with the top c-WO_3 intercalated (colored). a) First Cycle b) Second Cycle c) Third Cycle

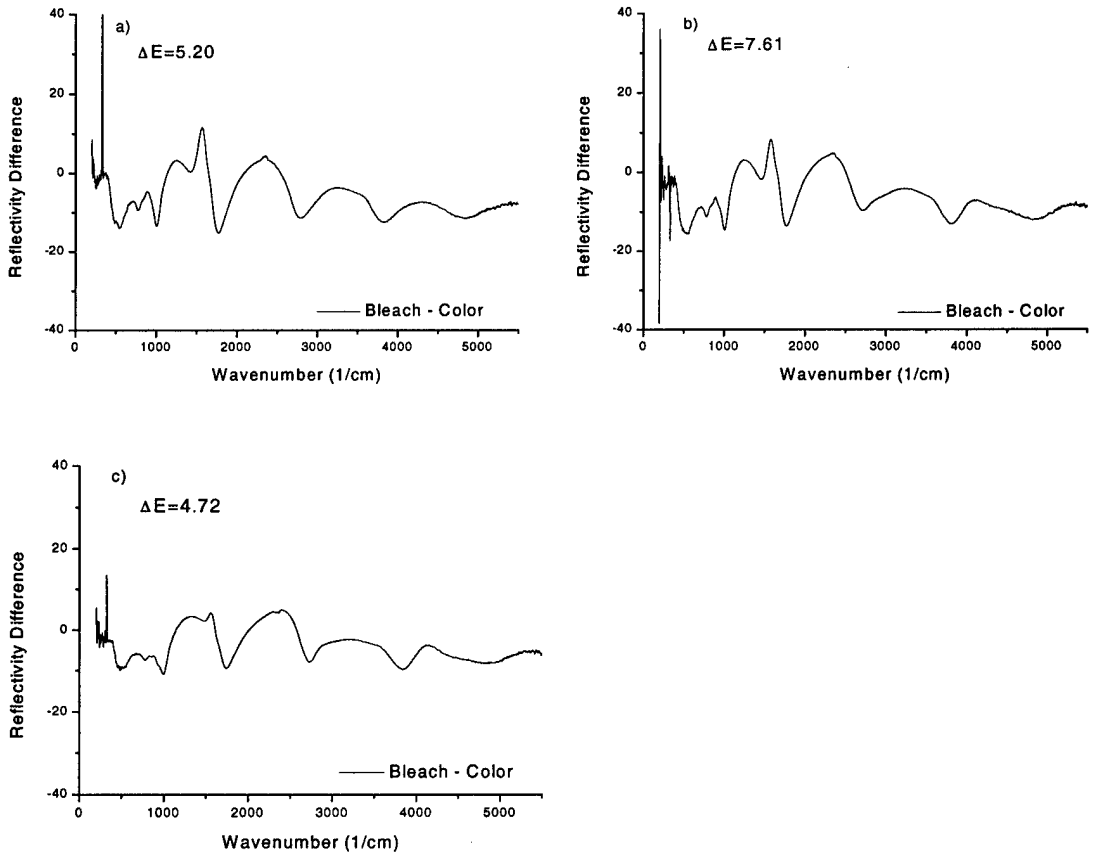

Figure 33: The difference in reflectance between the two operating states of Device #4 (Aluminum Conducting Grid). a) First Cycle b) Second Cycle c) Third Cycle

II) Device #5 (Aluminum Conducting Grid)

For this device 95% of the blackbody region was covered in the measurement.

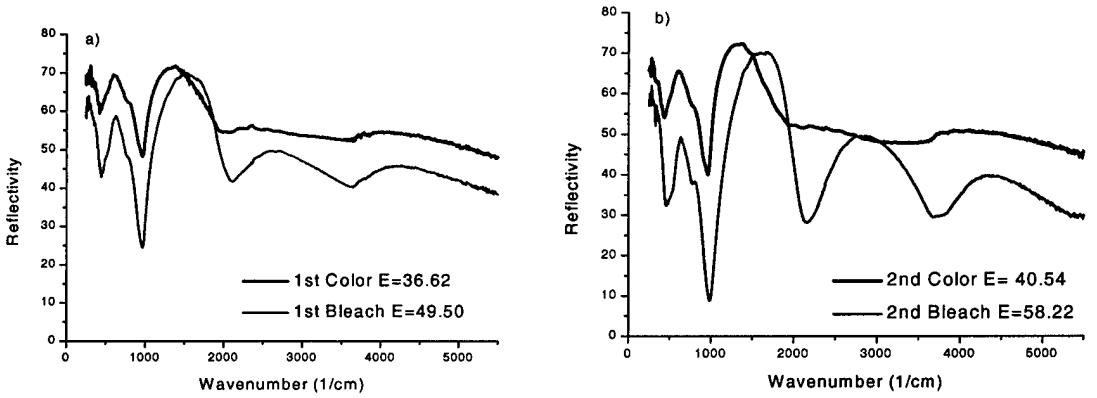

Figure 34: The measured reflectance of Device #5 (Aluminum Conducting Grid)$^{+}$——with the c-WO_3 unintercalated (bleached) and —— with the top c-WO_3 intercalated (colored). a) First Cycle b) Second Cycle

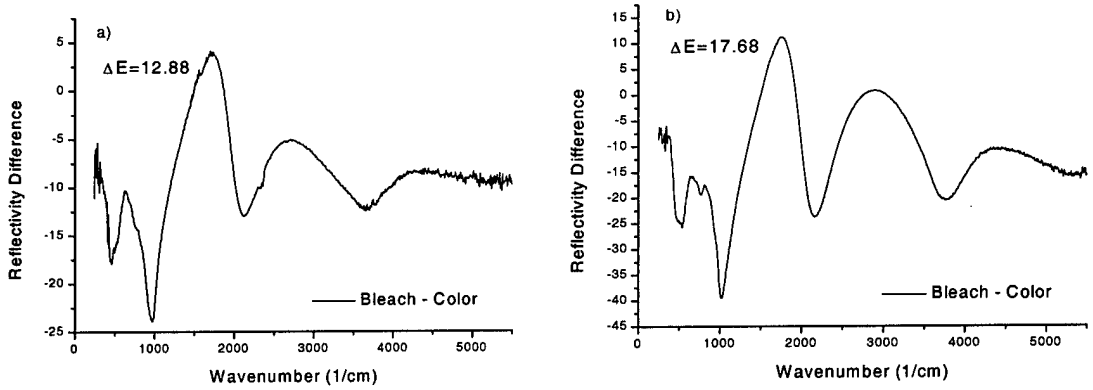

Figure 35: The difference in reflectance between the two operating states Device #5 (Aluminum Conducting Grid). a) First Cycle b) Second Cycle.

F) ALTERNATIVE ALL-VACUUM MONOLITHIC DEVICE FABRICATION METHODS

An important goal to device fabrication in this contract was to develop a method of intercalating the electrochromic layers with a vacuum compatible technique. It is well known that when an intercalant atom such as Li^+ is delivered to the surface of an electrochromic material it will diffuse into the film and still be reversibly extracted. We have developed an evaporation system that utilized Lithium foil as an evaporant (see quarterly report 4).

There are many benefits to a dry intercalation technique. The first is that there would be no damaging wet processes. Wet processes increase the chance of having pinhole shorts through the device and also induce more surface damage effects than dry techniques. The next benefit is that with a dry intercalation technique it is easy to develop a deposition method that would allow complete device fabrication without breaking vacuum. Lastly some of the materials are not compatible with the solvents used in wet intercalation methods.

A sample of c-WO_3 deposited on an ITO coated glass slide was vacuum intercalated with a Lithium metal evaporant. Two areas of the sample were tested, a region exposed to the Lithium and a region that was never exposed during the dry intercalation. Upon removing the sample from the chamber the exposed area was a deep uniform blue color, and the region that was not exposed was transparent. Visible transmission measurements were taken immediately after the sample was removed from the chamber. One measurement was made in the region that had not been exposed this is the As Deposited curve in figure 36, and one measurement was made in the region that had been exposed, the curve labeled Vacuum Intercalated shows this data.

After these measurements had been taken the sample was electrochemically colored and bleached several times. Finally a bleaching voltage was applied for a time that was sufficient enough to assume that any Li^+ ions that had been reversibly incorporated into the film had been removed. After this processing was complete two new transmission measurements were taken. The transmission data that was collected from the area that was not exposed to the dry intercalation processing is labeled on

figure 36 as Bleached Unexposed. The transmission data that was collected from the area that had been intercalated in the vacuum chamber is labeled as Bleached Exposed.

These data show that the evaporation-intercalated region had some lithium that was irreversibly intercalated into the film. It also demonstrates that this area could also be bleached out successfully. Although not as much as the region that had only been exposed to the electrochemical intercalation. With tighter control of the amount of Li atoms that are allowed to reach the surface of the sample the irreversible intercalation could be minimized.

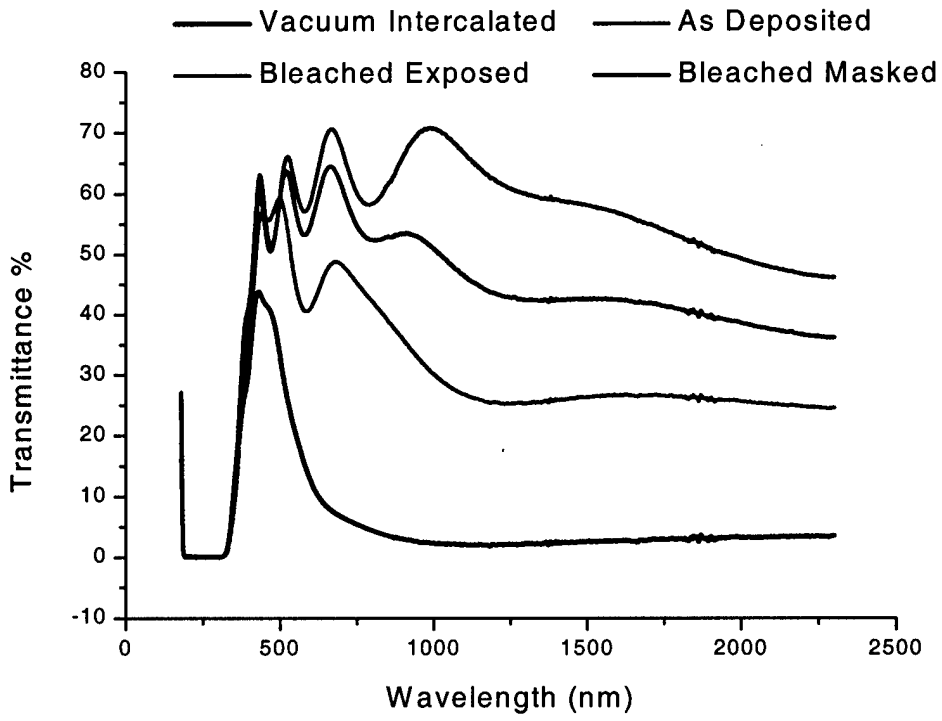

Figure 36: Transmittance data acquired from a vacuum intercalated sample of c-WO_3 on an ITO coated glass slide.

Table 2 Summary of Monolithic Device Performance.

Device Number	% Of Blackbody Covered	Cycle #	Emissivity with c-WO_3 Bleached	Emissivity with c-WO_3 Colored	Change in Emissivity	% Change in Emmissivity (relative to bleached)
Device #1	75	1	60.81	63.58	-2.77	-4.56%
		2	63.57	63.09	0.48	0.76%
		3	62.73	62.44	0.28	0.45%
Device #2	92	1	60.61	60.34	0.27	0.45%
		2	59.17	56.43	2.74	4.63%
Device #3 (Thin Conducting Top Layer)	92	1	7.05	25.35	-18.30	-259.57%
Device #4 (Aluminum Conducting Grid)	95	1	60.49	55.28	5.20	8.60%
		2	61.75	54.14	7.61	12.32%
		3	58.65	53.93	4.72	8.05%
Device #5 (Aluminum Conducting Grid)	95	1	49.50	36.62	12.88	26.02%
		2	58.22	40.54	17.68	30.37%

PART V: CONCLUSIONS

Many of the objectives for this contract have been met. The goal of extending IR measurement capabilities is foremost among them. This contract has assisted the J.A. Woollam Co. in developing an excellent product that has been shipped to commercial customers.

The goal of developing a dry method of intercalation has been met. This will insure manufacture of electrochromic devices will not require yield decreasing wet processing techniques.

Film uniformity was investigated by optical mapping techniques. It was determined that the area of the substrates that devices are manufactured on have uniformity that is more than adequate for fabrication.

In working towards durable long lifetime devices the use of Li^+ mobile ions was implemented. Also eliminating the polymer from the device has enhanced IR performance, manufacture feasibility, and potential space application durability.

This contract has also allowed the research institutions involved to make meaningful, relevant contributions to the electrochromics literature. Three articles have already been published and two more will be submitted for publication by the end of February 2000.

Extensive work has been done on c-WO_3 for its application to far infrared devices. Future work can use this information in determining the feasibility of using c-WO_3 in devices where IR modulation is desired. Utilizing a-WO_3 as a charge storage layer will cut down manufacturing time significantly when manufactured in high volume. Our work with Tantalum Oxide ion-conducting layers makes an important contribution to electrochromics research.

This contract has allowed us to determine the optical constants of many materials used for electrochromic devices including a-WO_3, c-WO_3, NiO, Tantalum Oxide, and ITO.

Many devices have been made which show significant IR emissivity modulation. The benefits of utilizing anti-reflective coatings have been demonstrated. The ability to utilize grid conductors has also been demonstrated. These are both important contributions to future IR electrochromic devices. We have developed what we believe is the first monolithic, all-vacuum processed IR electrochromic device. This is also the first time electrochromics have been measured over such a wide spectral range. Previous studies were limited to wavelengths shorter than 14μm.

There have also been some disappointments during the course of this contract. We have been unable to make long lifetime reliable electrochromic devices. Devices fail after only 3 or 4 switching cycles. This was the most difficult objective to meet and also the most important.

The second disappointment is that the emittance modulation of our devices is not high or reproducible. After making many devices, only near the end of the contract did we get devices with good modulation.

The biggest hurdle in making reliable devices has been the ion conducting layer. We have made tungsten oxide samples that are robust and durable in an electrochemical cell. All indications are that these films would be excellent in an IR operating device. The electrical conducting materials, such as ITO, Si, and thin metal layers, also have

properties that would make them suitable for an all vacuum fabricated electrochromic device. However, we have not been able to sputter deposit a good ion conductor that is electrically insulating. Most devices that we have made have electrical shorts between the two conducting layers. With electrons able to flow through the device no applied potential field will cause the modulation inducing ions to move into the desired films.

There are several possible reasons our measured device performance is not as great as the theoretical modulation predicted by single film studies. The Li^+ ions may be accumulating at interfacial sites between film layers. It is also likely that, at the interfaces, surface roughness contributes to light loss, due to scattering.

Without having made reliable small area devices two of the other contract objectives could not be met. We have not been able to explore large area devices, or devices which could be used on non-planar surfaces.

PART VI: RECOMMENDATIONS

There are several recommendations that should be considered for future work in IR electrochromics. It should also be noted that IR optical switches could be useful for applications other than room temperature blackbody emittance modulation. Electrochromics could find potential use for laser windows at IR wavelengths less than say 14μm. Perhaps space systems needing to be maintained at temperatures higher than 25°C could make use of devices like the ones made during this contract. The motivation for proposing this is that the shorter the wavelength, the better the WO-based electrochromic devices perform. The following figure shows the spectra for a body at 600K.

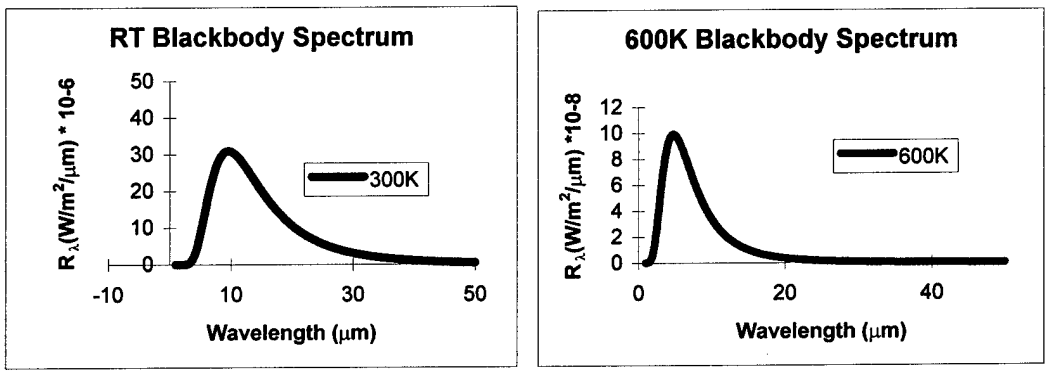

The peak of the radiation spectra from this body is shifted towards the shorter wavelengths, relative to the peak of a room temperature blackbody.

Electrochromic device research requires a good understanding of several disciplines. There is of course a need for a good optics background because these devices are designed to modulate light radiation in some way. There is also a need for a strong solid state physics and/or materials science background. The optical properties of all of these materials rely heavily on their structural properties. The fact that the cause of optical modulation is an intercalation of mobile ions into a host lattice is enough to make the need for a physics background desirable. Successful electrochromic devices behave analogously to solid state batteries. An electrochromics research program would benefit tremendously with an electrochemical research specialist. For a visible device program a

polymer chemist would also add an important contribution to an electrochromics research team. For visible devices polymers have many advantages over vacuum deposited materials.

Much thought should also be given to facilities requirements of an electrochromics research project. A clean room should be available. Particulates on substrates or on films that are going to have other materials deposited can induce pinhole shorts into the device. A small density of these pinholes will cause a device to fail. An oxygen free glove-box will be instrumental in carrying out meaningful electrochemical experiments. Lastly a good evaporation deposition system should be available to deposit the best ion conducting electrolyte films. Most of the successful visible devices are based on ceramic ion conductors, such as Aluminum Oxide or LiAlF, which are extremely difficult to sputter deposit. For these, an e-beam evaporator is highly desirable in any electrochromics development team. There are likely several other dielectrics that can be tried out for their ion conductivity and insulating properties. Hopefully one with low pinhole concentration can be found.

For spacecraft applications more work needs to be done on electrochromic materials and their durability in LEO environments. Simple experiments of c-WO_3 exposed to atomic oxygen show that the material undergoes irreversible color changes. Literature also suggests that under the influence of UV radiation WO_3 will also change its optical properties. Even with a successful emittance modulating IR device much work would need to be done to insure compatibility with the space environment.

REFERENCES

1. B. Johs, J.A. Woollam, C.M. Herzinger, J. Hilfiker, R. Synowicki, and C.L. Bungay, *Proceedings of Optical Metrology,* edited by G.A. Al-Jumaily, Bellingham, Washington, SPIE CR72, 1999, pp 29-56.

2. W.G. Spitzer, *Semiconductors and Semimetals vol. 3,* edited by R.K. Willardson, and A.C.Beer, New York, Academic Press, 1967, pp. 17-33.

3. J.A. Woollam, B. Johs, C.M. Herzinger, J. Hilfiker, R. Synowicki, C.L. Bungay, *Proceedings of Optical Metrology,* edited by G.A. Al-Jumaily, Bellingham, Washington, SPIE CR72, 1999, pp 3-28.

4. R.B. Goldner, F.O.Arntz,G. Berera, T.E. Haas, G.Wei, K.K. Wong and P.C. Yu, Solid state Ionics, 617 (1992), 53.

5. S.F. Cogan, T.D. Plante, M.A. Parker, and R.D. Rauh, J. Appl. Phys., 2735 (1986), 60.

6. P.C. Yu, D.L. Backfisch, N.A. O'Brien, and B.P. Hichwa, U.S. Patent No. 5,520,851

7. J.A. Woollam, X. Gao, S. Heckens, J.N. Hilfiker, in International Symposium on Polarization Analysis and Applications to Device Technology, T. Yoshizawa, H Yokota, (ed.), Proc. Soc. Photo-Opt. Instrum. Engr., Vol. 2873, Yokohama, Japan, (1996), 140.

8. M.S. Burdis, J.R. Siddle and S. Taylor, in Optical Materials Technology for Energy Efficiency and Solar Energy Conversion XIII, V. Wittwer, C. Granqvist and C. M. Lampert (ed.), Proc. Soc. Photo-Opt. Instrum. Engr., Vol. 2255, Freiburg, Federal Republic of Germany, (1994), 371.

9. C.M. Lampert, Vo-Van Truong and J. Nagai, Characterization Parameters and Test Methods for Electrochromic Device in Glazing Applications, International Energy Agency, Task X-C, glazing Materials, Interim Working Document LBL-29632.43e.

10. S.F. Cogan, E.J. Anderson, T.D. Plante and R.D. Rauh, in Optical Materials Technology for Energy Efficiency and Solar Energy Conversion IV, C.S. Lampert (ed) Proc. Soc. Photo-Opt. Instrum. Engr., Vol 562, 1985, 23.

11. W. Estrada, A.M. Andersson, C.G. Granqvist, J. Appl. Phys., 3678 (1988), 64.

12. A.J. Waldorf, J.A. Dobrowolski, B.T. Sullivan, and L.M. Plante, Appl. Opt. 32, 5583 (1993).

13. W.M. Paulson, F.S. Hickernell, and R.L. Davis, J. Vac. Sci. Technol. A 16, 307 (1979).

14. I. Proqueras, J. Marti, and E. Bertran, Thin Solid Films 343, 449 (1999).

15. M. Kitao, H. Akram, K. Urabe, and S. Yamada, J. Electronic Mater. 21, 419 (1992).

16. P.C. Joshi, and M.W. Cole, J. Appl. Phys. 86, 871 (1999).

17. A. Pignolet, G.M. Rao, and S.B. Krupanidhi, Thin Solid Films 258, 230 (1995).

18. S. Ezhilvalavan, and T.Y. Tseng, J. Am. Ceram. Soc. 82, 600 (1999).

19. S.W. Park, and H.B. Im, Thin Solid Films 207, 258 (1992).

20. V. Mikhaelashvili, Y. Betzer, I. Prudnikov, M. Orenstein, D. Ritter, and G. Eisenstein, J. Appl. Phys. 84, 6747 (1998).

21. F.C. Chiu, J.J. Wang, J.Y. Lee, and S.C. Wu, J. Appl. Phys. 81, 6911 (1997)

22. S.O. Kim, J.S. Byun, and H.J. Kim, Thin Solid Films 206, 102 (1991).

23. S.W. Park, Y.K. Baek, J.Y. Lee, C.O. Park, and H.B. Im, J. Electr. Mat. 21, 635 (1992).

24. C. Chaneliere, S. Four, J.L. Autran, R.A.B. Devine, and N.P. Sandler, J. Appl. Phys. 83, 4823 (1998).

25. B.K. Moon, C. Isobe, and J. Aoyama, J. Appl. Phys. 85, 1731 (1999).

26. I. Kim, J.S. Kim, O.S. Kwon, S.T. Ahn, J.S. Chun, and W.J. Lee, J. Electronic Materials 24, 1435 (1995).

27. R.A.B. Devine, L. Vallier, J.L. Autran, P. Paillet, and J.L. Leray, Appl. Phys. Lett. 68, 1775 (1996).

28. M. Schubert, B. Rheinländer, E. Franke, H. Neumann, J. Hahn, M. Röder, and F. Richter, Appl. Phys. Lett. 70, 1819 (1997).

29. M. Schubert, B. Rheinländer, E. Franke, H. Neumann, T.E. Tiwald, J.A. Woollam, J. Hahn, and F. Richter, Phys. Rev. B 56, 13306 (1997).

30. E. Franke, M. Schubert, H. Neumann, T.E. Tiwald, D.W. Thompson, J.A.

31. Woollam, J. Hahn, and F. Richter, J. Appl. Phys. 82, 2906 (1997).

32. E. Franke, M. Schubert, J.-D. Hecht, H. Neumann, T.E. Tiwald, H. Yao, J.A. Woollam, and J. Hahn, J. Appl. Phys. 84, 526 (1998).

33. M. Cevro, and G. Carter, Opt. Engineer 34, 603 (1995).

34. H. Demiryont, J.R. Sites, and K. Gelb, Appl. Opt. 24, 490 (1985).

35. W.B. Westwood, R.J. Boynton, and S.J. Ingrey, J. Vac. Sci. Technol. 11, 381 (1974).

36. X.H. Pan, S.L. Qiu, M.I. Florit, M.L. Shek, and M. Strongin, Phys. Rev. B 35, 3740 (1987).

37. D.J. Werder, and R.R. Kola, Thin Solid Films 323, 6 (1998).

38. K. Gürtler, K. Bange, W.Wagner, F. Rauch, and H. Hantsche, Thin Solid Films 175, 185 (1989).

39. Y. Nishimura, A. Shinkawa, H. Ujita, M. Tsuji, and M. Nakamura, Appl. Surf. Sci. 136, 22 (1998).

40. Z.W. Fu, L.Y. Chen, and Q.Z. Qin, Thin Solid Films 340, 164 (1999).

41. G.B. Alers, R.M. Fleming, Y.H. Wong, B. Dennis, A. Pinczuk, G. Redinbo, R. Urdahl, E. Ong, and Z. Hasan, Appl. Phys. Lett. 72, 1308 (1998).

42. J.Y. Zhang, B. Lim, and I.W. Boyd, Thin Solid Films 336, 340 (1998).

43. J.Y. Zhang, B. Lim, and I.W. Boyd, Appl. Phys. Lett. 73, 2299 (1998).

44. K. Kukli, J. Aarik, A. Aidla, O. Kohan, T. Uustare, and V. Sammelselg, Thin Solid Films 260, 135 (1995).

45. D. Laviale, J.C. Oberlin, and R.A.B. Devine, Appl. Phys. Lett. 65, 2021 (1994).

46. J. Hodgkinson, Q.H. Wu, and J. Hazel, Appl. Opt. 37, 2653 (1998).

47. D. Aspnes. and J.B. Theeten, Phys. Rev. B 20, 3292 (1979).

48. R.M.A. Azzam, and N.M. Bashara, *Ellipsometry and Polarized Light*, (North-Holland, Amsterdam, 1977).

49. G.E. Jellison, Thin Solid Films 313-314, 33 (1998).

50. C.M. Herzinger, B. Johs, W.A. McGahan, J.A. Woollam, and W. Paulson, J. Appl. Phys. 83, 3323 (1998).

51. E.D. Palik, *Handbook of optical constant of Solids* (Academic Press, New York, 1998).

52. T.E. Tiwald, D.W. Thompson, J.A. Woollam, and S.V. Pepper, Thin Solid Films 313-314, 718 (1998).

53. C.M. Herzinger, P.G. Snyder, B. Johs, and J.A. Woollam, J. Appl. Phys. 77, 1715 (1995).

54. C.M. Herzinger, H. Yao, P.G. Snyder, F.G. Celii, Y.C. Kao B. Johs, and J.A. Woollam, J. Appl. Phys. 77, 4677 (1995).

55. *Guide to use WVASE 32*, J.A. Woollam Co., Inc. Lincoln, (1995).

56. S. Zollner, Appl. Phys. Lett. 63, 2523 (1993).

57. M. Schubert, J.A. Woollam, G. Leibiger, B. Rheinländer, I. Pietzonka, T. Sass, and V. Gottschalch, J. Appl. Phys. 86, 2025 (1999).

58. C.C. Kim, J.W. Garland, H. Abad, and P.M. Raccah, Phys. Rev. B 45, 11749 (1992).

59. C.C. Kim, J.W. Garland, and P.M. Raccah, Phys. Rev. B 47, 1876 (1993).

60. J.W. Garland, C. Kim, H. Abad, and P.M. Raccah, Phys. Rev. B 41, 7602 (1990).

61. C.M. Herzinger, and B.D. Johs, Patent 5796983 (1998).

62. M. Schubert, T.E. Tiwald, C.M. Herzinger, Phys. Rev. B 61 (2000).

63. A. Kasic, M. Schubert, S. Einfeldt, D. Hommel, unpublished.

64. D. G. Gilmore, Satellite Thermal Control Handbook (The Aerospace Corporation Press, El Segundo, California, 1994), pp. 4-101.

65. S. K. Deb, Philos. Mag. 27, 801-822, (1973).

66. J. S.Hale, M. J. DeVries, B. Dworak, J. A. Woollam, Thin Solid Films 313-314, 205-209, 1998.

67. S. F. Cogan, R. D. Rauh, J. D. Klein, and T. D. Plante, in Proceedings on the Symposium on Electrochromic Materials II, edited by Kuo-Chuan Ho and Donald A. MacArthur (The Electrochemical Society, Pennington, NJ, 1994), pp. 269-277.

68. R. B. Goldner, F. O. Arntz, K. Dickson, M. A. Goldner, T. E. Haas, T. Y. Liu, S. Slaven, G. Wei, K. K. Wong, P. Zerigian, in Proceedings on the Symposium on Electrochromic Materials II, edited by Kuo-Chuan Ho and Donald A. MacArthur (The Electrochemical Society, Pennington, NJ, 1994), pp. 237-243.

69. R. B. Goldner and R. D. Rauh, Proc. Soc. Photo-Opt. Instrum. Engr. 428, 38-44 (1983).

70. H. J. Byker, in Proceedings on the Symposium on Electrochromic Materials II, edited by Kuo-Chuan Ho and Donald A. MacArthur (The Electrochemical Society, Pennington, NJ, 1994), pp. 3-13.

71. P. M. S. Monk, R. J. Mortimer, D. R. Rosseinsky, Electrochromism: Fundamentals and Applications (VCH, Weinheim, FRG, 1995), pp. 67-68.

72. R. B. Goldner, in Solid State Ionic Devices, edited by B. V. R. Chowdari and S. Radhakrishna (World Scientific Publishing Co., Singapore, 1988), pp. 379-390.

73. R. D. Varjian, M. Shabrang, S. J. Babinec, in Proceedings on the Symposium on Electrochromic Materials II, edited by Kuo-Chuan Ho and Donald A. MacArthur (The Electrochemical Society, Pennington, NJ, 1994), pp. 278-289.

74. K. Bange, C. Ottermann, W. Wagner, F. Rauch, in Large Area Chromogenics: Materials and Devices for Transmittance Control, edited by C. M. Lampert and C. G. Granqvist (SPIE Opt. Engr. Press, Bellingham, 1990), pp. 122-128.

75. Jeffrey S. Hale, MSEE thesis, University of Nebraska-Lincoln, 1997.

76. C. G. Granqvist, Handbook of Inorganic Electrochromic Materials (Elsevier, Amsterdam, The Netherlands, 1995), p. 59.

77. P. Drude, The Theory of Optics, translated by C. R. Mann and R. A. Millikan (Longmans, Green and Co., New York, 1933) pp. 396-399.

78. C. Kittel, Introduction to Solid State Physics, 6th ed. (Wiley, New York, 1986), p. 50.

79. D. Grier, G. McCarthy, XRD data (International Centre for Diffraction Data, Newton Square, PA, 1992).

80. Q. Zhong, J. R. Dahn, and K. Colbow, Phys. Rev. B 46, 2554-2560 (1992).

81. H. Kaneko, F. Nagao, K. Miyake, J. Appl. Phys. 63, 510-517, 1988.

82. F. Wooten, Optical Properties of Solids (Academic Press, Inc., USA, 1972).

83. Guide to Using WVASE32 (J. A. Woollam Co., Inc.; Lincoln, NE; 1995).

84. M. Kitao, H. Akram, K. Urabe, S. Yamada, J. Electronic Mater. 21, 419-422 (1992).

85. Y. Hajimoto, M. Matsushima, S. Ogura, J. Electronic Mater. 8, 301-310 (1979).

86. B. P. Hichwa, G. Caskey, D. F. Betz, J. D. Harlow, J. Vac. Sci. Technol. A 5, 1775-1777 (1987).

87. M. L. Lieberman, R. C. Medrud, J.Electrochem. Soc. 116, 242-247 (1969).

88. F. Rubio, J. Vac. Sci. Technol. 21, 1043-1045 (1982).

89. P. C. Yu, D. L. Backfisch, N. A. O'Brien, and B. P. Hichwa, U. S. Patent Number No. 5,520,851 (28 May 1996).

90. R.B. Goldner, F. Arntz, G. Berera, T.E. Haas, G. Wei, K.K. Wong, and P. Yu, Proc. SPIE 1536, 34 (1991).

91. S.F. Cogan, R.D. Rauh, J.D. Klein, and T.D. Plante, Proc. SPIE 1149, 2 (1989).

92. K. Baucke, Solar Energy Mater. 16, 67 (1987).

93. P. Topart, and P Hourquebie, Thin Solid Films 352, 243 (1999).

94. C.L. Trimble, M.J. DeVries, J.S. Hale, D.W. Thompson, T.E. Tiwald, and J.A. Woollam, Thin Solid Films 347, 1 (1999).

95. J.S. Hale, and J.A. Woollam, Thin Solid Films 339, 174 (1999).

96. M.J. DeVries, C.L. Trimble, T.E. Tiwald, D.W. Thompson, J.A. Woollam, and J.S. Hale, J. Vac. Sci. Technol. A 17(5), 2906 (1999).

97. E. Franke, M. Schubert, C.L. Trimble, M.J. DeVries, J.S. Hale J.A. Woollam, and F. Frost, submitted to J. Appl. Phys.

98. J.S. Hale, M.J. DeVries, B. Dworak and J.A. Woollam, Thin Solid Films 313-314, 205 (1998).

Scientific & Technical Reports Summary
Final Report

Spacecraft Thermal Control Management Using Electrochromics
#DASG60-98-C-0054
Contract Remarks

The J.A. Woolam Co. Inc, as the contractor, concludes at the completion of the contract (#DASG60-98-C-0054) that the processes involved in this research and experimentation do not involve any hazardous materials or hazardous control procedures. In addition, there have been no prototype devices successfully fabricated by the end of this research.